Carbohydrate Polymer Technologies and Applications 8 (2024) 100575

Contents lists available at ScienceDirect

Carbohydrate Polymer Technologies and Applications

journal homepage: www.sciencedirect.com/journal/carbohydrate-polymer-technologies-and-applications

Gelatin-based ballistic gel formulated with phytosynthesized nanocellulose from *Arundo donax* for alpha-amylase enzyme inhibition activity

Jaison Jeevanandam, Rita Castro, João Rodrigues *

CQM - Centro de Química da Madeira, MMRG, Universidade da Madeira, Campus da Penteada, 9020-105, Funchal, Portugal

ARTICLE INFO

Keywords:
Invasive plant
Nanocellulose
Hydrogel
Antidiabetic activity
Amylase inhibition

ABSTRACT

Arundo donax, an indigenous plant in the Mediterranean region, has affected the growth of native vegetation as an invasive plant, ultimately reducing soil quality and affecting the food chain in several areas of the world. Thus, the present work aims to obtain cellulose from the *A. donax* leaf extract via organosolv fractionation and bleaching method, followed by centrifugal fractionation to yield nanocellulose of moderately monodispersed (0.428 PDI) 91.2 nm in size and a zeta potential of -35.5 mV of high stability in aqueous medium (water). In addition, the resultant nanocellulose was formulated in ballistic gelatin hydrogel, and their antidiabetic effect via alpha-amylase enzyme inhibition activity was also investigated. Systematic characterization of the hydrogel samples (different volume ratios of gelatin and nanocellulose) revealed that the sample with 18:2 (v/v) gelatin: nanocellulose content is thermally stable until 152 °C, releasing nanocellulose for three days from hydrogel until 45 °C. This study confirms the feasibility and potential of utilizing invasive plant species to extract nanocellulose for medical purposes. Furthermore, the gelatin-formulated nanocellulose, with its demonstrated alpha-amylase inhibition activity at a dosage of 80 μg/mL, holds the promise of being a potential revolutionary medical gummy for sustained reduction of blood glucose levels.

1. Introduction

Cellulose $(C_6H_{10}O_5)_n$ is an organic polysaccharide compound with a linear chain of several beta-linked glucose units Mathura & Maharaj (2024); Reddy & Yang (2005). The high natural biodegradability, biocompatibility, hydrophilicity, and nontoxicity of cellulose make it a significant material for desired medical applications, such as tissue engineering, blood purification, hemostatic agent, hepatocyte culture material, wound dressing, enzyme inhibitor, post-operative adhesion barrier, and controlled drug delivery system Dhital, Gidley, & Warren (2015); More, Antanitta. S, Khonde, & Kandasubramanian (2024); Sindhu, Prasanth, & Thakur (2014). Plants and bacteria (vascular plants, cotton, jute, corn, rice, *Agrobacterium, Sarcina ventriculi*, and genera *Acetobacter*) are the primary sources of cellulose, where the cell walls of plants possess cellulose to provide structural integrity Gorgieva & Trček (2019); Heinze, El Seoud, & Koschella (2018); Mohamad Amini (2024). However, pure cellulose lacks mechanical and thermal stability, and hence, researchers are in a quest to identify a novel alternative for cellulose. Consequently, nanocellulose is being explored as a potential replacement for conventional cellulose due to its high thermal and mechanical stability, reinforcing capability, and self-assembly in aqueous dispersion media, along with enhanced biodegradability, nontoxicity, and low density Sharma et al. (2021). Nanocellulose is currently prepared via pretreatment methods, followed by physical or chemical approaches. For instance, enzyme hydrolysis, ionic liquids, and alkaline/acid can be used for the pretreatment of cellulose. Mechanical treatments, including high-pressure homogenization, microfluidization, cryocrushing, grinding, ball milling, and high-intensity ultrasonication, are common physical approaches. In contrast, chemical approaches, such as 2,2,6,6-tetramethylpiperidinyloxy (TEMPO) oxidation and sulfuric acid hydrolysis, were widely utilized for nanocellulose preparation Nasir, Hashim, Sulaiman, & Asim (2017); Yang, Ullah, & Zhijun (2021). The mechanical methods help in the defibrillation process of cellulosic materials Chauhan & Chakrabarti (2012) while chemical approaches will lead to increased inner surface, hydroxyl group space widening, disruption of hydrogen bonds of cellulose, and alteration of their crystallinity Amaral-Labat et al. (2012); Kassie, Daget, & Tassew (2024). However, mechanical approaches require costly equipment and maintenance, which eventually affects the downstream processing of nanocellulose (Balea et al., 2021; Dhali, Ghasemlou,

* Corresponding author.
E-mail addresses: joaoc@staff.uma.pt, joaor@uma.pt (J. Rodrigues).

https://doi.org/10.1016/j.carpta.2024.100575

Available online 24 September 2024

Daver, Cass, & Adhikari, 2021), whereas chemical methods involve hazardous chemicals that can lead to toxicity challenges Afrin & Karim (2017). Thus, a novel approach is needed to extract cellulose and form nanocellulose from exclusive plant sources.

Arundo donax is a large perennial grass that is native to temperate and tropical regions and is widely distributed in the Mediterranean region Jepson (1993); Kassem, Ali, & Saad Zaghloul (2024). After 1960, this plant was introduced to Europe and has since become widely dispersed as an invasive species in Mexico, the Pacific islands, the Caribbean, southern Africa, South America, and the subtropical USA Hafliger & Scholz (1981); Ozudogru, Karlik, Elazab, & Lambardi (2023). *A. donax*, as an invasive plant, has affected the growth of native vegetation, which eventually reduces the soil quality and affects the food chain in the region Amarone et al. (2023); Randall (2012). In general, these invasive plants are removed from the environment via mechanical (mowing, tilling) (Nunez-Gonzalez, Rodriguez, & Gonzalez, 2021), chemical (pesticides) (Eigenbrode et al., 2008; Hinkson et al., 2024), and biological (insect predators or plant diseases) approaches Driesche & Center (2013); Hameed et al. (2024). Each of these approaches also possesses various limitations, including costs involved, time, and reduction in soil quality Weidlich, Flórido, Sorrini, & Brancalion (2020). Until now, there has been no process to reuse the phytochemicals present in these invasive plants, which will reduce their spread and be beneficial for the desired application Jeevanandam & Rodrigues (2024). It is noteworthy that *A. donax* possesses 35 % of hemicellulose, 31 % of cellulose, and 18 % of lignin Martínez-Sanz, Erboz, Fontes, & López-Rubio, (2018), which makes it a better source of cellulose compared to other invasive plant sources. Extraction of cellulose from *A. donax* will also help to reduce their population in the invaded environment and reuse them as a green source for nanocellulose production instead of depending on plants with medicinal or economic significance Bessa, Tarchoun, Trache, & Derradji (2021); Pires et al. (2022). Recently, alkaline-acid, alkali-silane, and acid hydrolysis treatments have been utilized for the extraction of cellulosic fibers and microcrystalline cellulose from the *A. donax* plant Bessa et al. (2021); Bessa et al. (2020); Gaikwad, Debnath, & Gupta (2023). It is noteworthy that, to our knowledge, only one previous study has reported the formation of nanocellulose from *A. donax* via alkali pre-treatment, bleaching, and acid hydrolysis. The major limitation of the study is the usage of high acid concentrations during preparation and the larger size of the nanocellulose Pires et al. (2022).

Recently, several studies identified that nanocellulose possesses antidiabetic activity by inhibiting the amylase enzyme , which is essential for converting of carbohydrates and starch into glucose, fructose, or maltose Afrin & Karim (2017); Liu & Kong (2021); Nsor--Atindana, Yu, Goff, Chen, & Zhong (2020). However, complete or irregular inhibition of such enzymes will eventually lead to low glucose levels in diabetic patients Alam & Mohd (2019); Yan, Zhao, Yang, & Zhao (2019). Hence, a controlled approach is required to release nanocellulose and inhibit amylase activity. Gelatin has been used as a formulation material for plant-based phytochemicals and utilized as nutraceuticals to improve their significant biological efficacies Bermudez-Beltrán, Marzal-Bolaño, Olivera-Martínez, & Espitia (2020); Esmaeili, Dayani, Taheri, & Zolfaghari (2021); Gómez-Mascaraque & Lopez-Rubio (2020). Further, gelatin has been used to formulate phytochemicals into gummies to enhance their biological applications (Martínez-Sanz et al., 2018; Pires et al., 2022), especially their enzyme inhibition activity, which improves their antidiabetic activity (Kavimughil, Leena, Moses & Anandharamakrishnan, 2022; Zhang, Cavender, & Allen, 2020). Thus, the present work aims to obtain cellulose from *A. donax* leaf extract via organosolv, bleaching, and calcination methods, followed by centrifugal fractionation to yield nanocellulose. Organosolv is a process of extracting lignin and cellulose using aliphatic or aromatic alcohols under the influence of an acid catalyst Islam, Sinha, and Prasad (2024). Likewise, bleaching is the process to eliminate impurities from the cellulose (Walawska, Olak-Kucharczyk, Kaczmarek, & Kudzin, 2024), and calcination is a thermal process to heat solid chemical compounds at their glass transition temperature in a controlled environment (Boonprasertpoh et al., 2024), which was utilized in this study for alpha-cellulose formation. In addition, the resultant nanocelluloses were formulated into ballistic gelatin hydrogel (prepared with high gelatin concentration) for high rigidity in room conditions, and their antidiabetic effect via alpha-amylase enzyme inhibition activity was also investigated. The significant innovation in this study is the development of nanocellulose by extracting and synthesizing it from invasive plants using a modified organosolv and bleaching method. This process aims to reduce the production of hazardous chemical byproducts. The nanocellulose is then added to a gelatin hydrogel to enhance its potential antidiabetic activity, which is a first-time achievement.

2. Experimental procedure

2.1. Materials

The dried leaf powder of *Arundo donax* was obtained from the Azores archipelago, Portugal (coordinates: 37.7804° N, 25.4970° W), which has been identified as an invasive plant in the Macaronesia region, affecting the local plant growth. The powder was dried in a bio-dryer and sieved using a 2-micron mesh to have a uniform size. Chemicals, such as ethanol (purity = 96%), 0.05 M of sulfuric acid (purity = 97%), 2% hydrogen peroxide (purity = 70%), and 8% sodium carbonate (purity = 99.8%) were procured from Riedel-de Haën (Germany), Chem-Lab (Belgium), Merck® (Portugal) and Sigma-Aldrich® (Germany), respectively. Further, gelatin from porcine skin (10 kDa) was purchased from Honeywell Fluka analytical™ (Portugal). Moreover, chemicals required for amylase enzyme inhibition activity were obtained from Sigma-Aldrich® (Germany) and Merck® (Portugal). Human saliva-derived lyophilized alpha-amylase enzyme procured from Sigma Aldrich® was used for alpha-amylase inhibition activity identification of nanocellulose and gelatin-formulated nanocellulose samples. All the chemicals (ethanol, sulfuric acid, hydrogen peroxide, sodium carbonate, gelatin, and alpha-amylase enzyme) were utilized in the experiment without any further purification, and all solutions (sulfuric acid, hydrogen peroxide, sodium carbonate, and gelatin) were prepared in water.

2.2. Extraction of cellulose and synthesis of nanocellulose

In the present study, the experimental procedure followed by Luo et al. was utilized for the extraction of cellulose from *Arundo donax* leaf powder with certain modifications Luo et al. (2019). Initially, 3 g of *Arundo donax* dried leaf powder was mixed with a 1:1:1 vol ratio of ethanol, ultrapure water, and sulfuric acid (0.05 M), which was then thermally treated in a muffle furnace (*Nabertherm® LVT5/11 muffle furnace*) at 150 °C for 6 h with a heating rate of 10 °C/min. Then the samples were dried at 50 °C (heating rate = 10 °C/min) for 16 h to yield an impure cellulose sample. In the next step, 2 g of impure cellulose sample was mixed with a 1:1 vol ratio of 2% hydrogen peroxide and 8% sodium carbonate, which was thermally treated in a muffle furnace for 24 h at 60 °C and dried at 50 °C for 24 h (heating rate = 10 °C/min) to yield pure cellulose complex. The resultant pure cellulose complex was centrifuged with ultrapure water for washing to yield pure cellulose complex powder. Furthermore, the cellulose complex was subjected to calcination at 200 °C for 2 h (5 °C/min) in a muffle furnace to yield pure cellulose. Centrifugal fractionation process using a *Sigma 3K30* centrifuge was utilized to separate smaller-sized cellulose particles from larger cellulose particles Zhai, Kim, Kim, and Kim (2020). The process of centrifugal fractionation was optimized via systematic characterization, such as dynamic light scattering (*Malvern NanoZS*) as well as UV–Visible spectroscopy (*PerkinElmer® Lambda 35*) and established to be 8050 g of centrifugation relative centrifugal force (RCF) for 20 min (refer supplementary information **Section S.5**), which yielded smaller-sized

nanocellulose particles, as shown in Fig. 1.

2.3. Characterization of cellulose and nanocellulose

The extraction of cellulose and formation of nanocellulose from the plant material were analyzed to confirm their crystallinity as well as their thermal property in each stage via X-ray diffractometer (XRD – *Bruker® D8 Advance*) and Thermogravimetry-Differential Thermal Analysis (TG-DTA; *NETZSCH STA 409 PC/PG*). 0.3 g of the powder samples were added to the sample holder, leveled, and loaded into the XRD equipment, where diffraction was performed from 0 to 180° via copper Kα as the X-ray source with a wavelength of 1.83 Å to analyze their crystallinity. Likewise, 20 mg of powder samples were loaded into the alumina crucible and placed into the TG-DTA with a temperature program to reach 500 °C at a rate of 5 °C/min. Further, the optical properties of the impure cellulose, pure cellulose complex, pure cellulose, and nanocellulose were identified via Ultraviolet-visible spectroscopy (UV–Vis; *PerkinElmer® Lambda 35*). 1 mg of powder samples was suspended in ultrapure water using a sonication method (*Phoenix 4.5 L digital ultrasonic cleaner*) at room temperature for 20 min. Later, the sample suspensions (2 mL) were transferred to glass cuvettes and placed in a UV–Vis spectrometer to measure their optical property from 200 to 800 nm at 1 nm wavelength intervals. Furthermore, the average particle size, polydispersity index and zeta potential, functional groups, and morphology/elemental analysis of the cellulose and nanocellulose were characterized via Dynamic/Electrophoretic Light Scattering (DLS/ELS, *Malvern NanoZS*), Fourier transform infrared spectroscopy (FTIR; *PerkinElmer® Spectrum Two*), Scanning Electron Microscopy with Energy-Dispersive X-Ray Spectroscopy (SEM, EDS; *Bench SEM Phenom ProX*), respectively. The same sample suspension approach as mentioned for optical property analysis was utilized for DLS/ELS, FTIR, and SEM analysis. 2 mL of the suspensions were loaded in a polystyrene latex cuvette (refractive index – 1.59 and light absorption of 0.01) and provided information about dispersant as water (temperature – 25 °C, viscosity – 0.8872 cP and refractive index – 1.330) for DLS/ELS analysis. More information about sample analysis via FTIR and SEM equipment was included in Sections 3.5 and 3.7.

2.4. Gelatin ballistic hydrogel formulation of nanocellulose

In the present work, 6 g of gelatin powder was mixed with 30 mL of ultrapure water and stored at 4 °C for 4 h for the preparation of virgin gel. Later, the virgin gel was melted in boiling water (~50 mL), which was further mixed with distinct concentrations (gelatin to nanocellulose volume ratio - 18:2, 16:4, 14:6, 12:8, 10:10) of colloidal nanocellulose to make the final solution into 20 mL. The gel was cast in a Petri dish, which was stored at 4 °C for 16 h to form ballistic nanocellulose-gelatin gel. The resultant nanocellulose gel formulation was cut into 1 × 1 cm small pieces and maintained at 4 °C for further analysis, as displayed in Fig. 2. Semba, Mieloch, Tomaszewska, Cywoniuk, & Rybka (2023); Yin, Ahmad, & Amin (2015).

2.5. Enzyme inhibition assay

The standard calibration curve of maltose, as displayed in the supplementary material (**Figure S.1)**, was obtained using an aqueous solution of 2 mg/mL of soluble maltose. In this study, different dosages of colloidal nanocellulose (60 mM of 20–100 µL) and gelatin-formulated nanocellulose (20–100 µg) were added to the sodium chloride (1%), amylase enzyme (40 U/mL in 1:20 dilution with water), and starch mixture (1 g of soluble starch in 200 mL of 0.1 M phosphate buffer at pH 6.8) for the identification of nanocellulose/gelatin-formulated

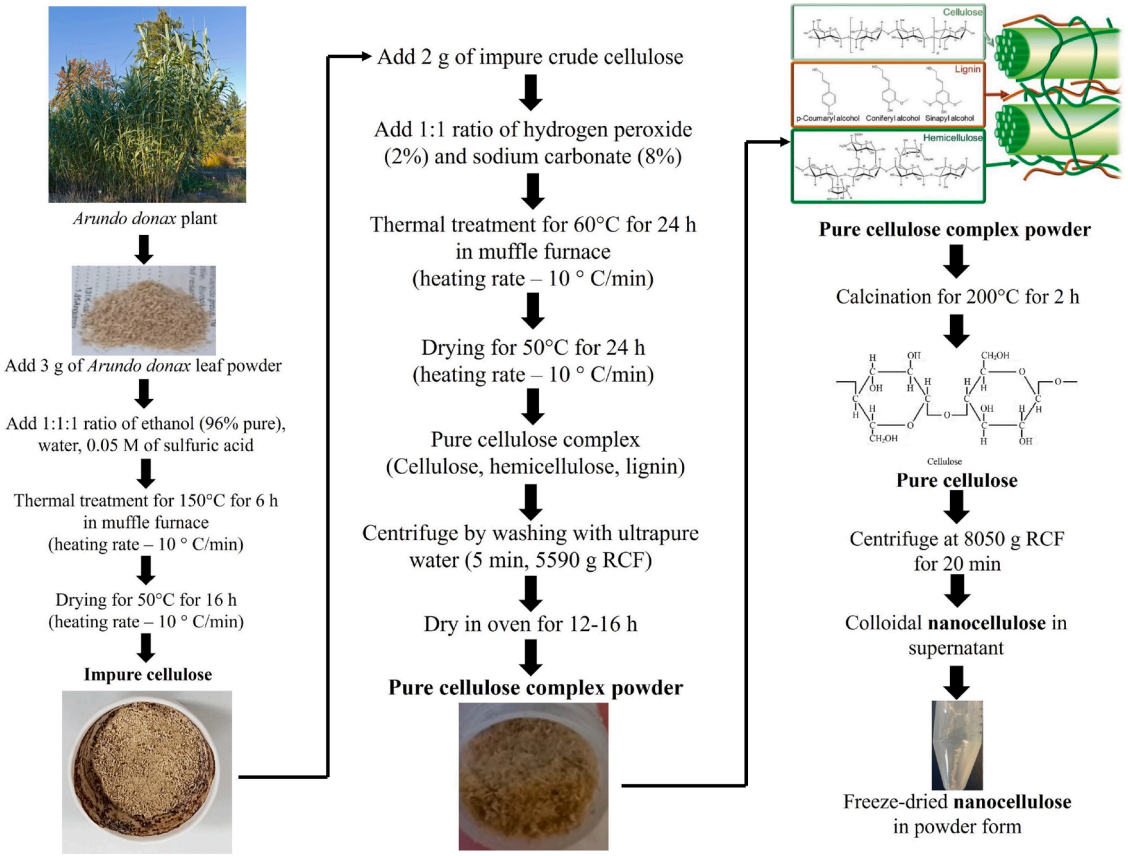

Fig. 1. Schematic flowchart of impure cellulose extraction using organosolv process, pure cellulose complex using bleaching approach, calcination to yield pure cellulose, and fractional centrifugation to form nanocellulose.

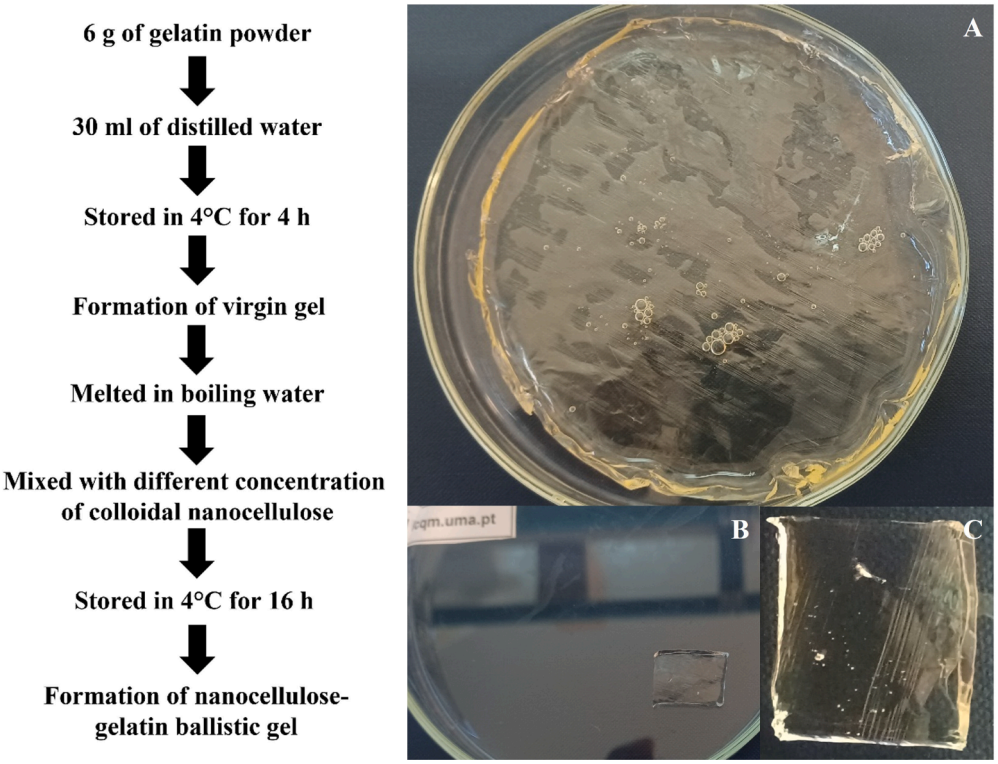

Fig. 2. Gelatin ballistic hydrogel formulation of nanocellulose extracted and fabricated from non-native *A. donax* leaf powder. Nanocellulose-gelatin ballistic gel (A) on Petri dish after preparation, (B) 1 × 1 cm cut piece, and (C) detailed view of the hydrogel.

nanocellulose dosage (standard calibration curve of maltose in **Figure S.1**) with high enzyme inhibition activity. The maltose concentration present in the test sample mixtures was identified by measuring its optical density (OD) value at 520 nm and substituted in the standard maltose graph. Control-sample/control x 100% is the formula utilized to determine the enzyme inhibition percentage of the nanocellulose and gelatin-formulated nanocellulose after 0 h and 24 h Ammulu et al. (2021).

3. Results and discussion

3.0.1. Color of the samples

It has been observed that the yellow color of the leaf powder has turned pale yellow due to the addition of ethanol and sulfuric acid during the organosolv process. Later, the pale-yellow color of the acidic crude leaf powder was intensified due to the addition of hydrogen peroxide and sodium carbonate solutions in the bleaching process. After the bleaching process, the resultant powder samples were subjected to calcination at 200 °C for 2 h to eliminate hemicellulose and lignin to yield pure cellulose powder (pale, whitish-yellow color) Carrier et al. (2011). Further, the resultant pure cellulose was fractionally centrifuged in deionized water (10 mg/mL) at 8050 g RCF to form cellulose nanoparticles by eliminating larger-sized particles (Zhai et al., 2020), which was freeze-dried to obtain cellulose nanoparticle powders (white powders).

3.0.2. pH of the samples

The pH of the leaf powder in the aqueous solution was identified to be 7.2, which was then reduced to 4.4 in the organosolv process due to the inclusion of sulfuric acid. Acidification has led to the degradation of certain phytochemicals, which has yielded an acidic cellulose complex (containing cellulose, hemicellulose, and lignin) Brosse, Hussin, & Rahim (2019). Further, the bleaching process has resulted in a powder with a neutral pH (~7). The bleaching process helps to reduce acidity in the leaf powder, eliminate unnecessary phytocompounds, and yield a neutral cellulose complex that is beneficial for biomedical applications Luo et al. (2019); Shatalov & Pereira (2005). Later, the pH of the calcined samples that resulted in pure cellulose and the nanocellulose after fractional centrifugation was identified to be neutral (~7).

All these observations have been primarily confirmed via systematic characterization methods, such as TG-DTA and XRD.

3.1. Thermal analysis of cellulose particles

Fig. 3 shows the TG-DTA analysis of plant leaf powder, impure cellulose complex, cellulose complex, and pure cellulose powder from 25 to 500 °C. Table 1 summarizes the cellulose sample's TG-DTA weight loss corresponding to temperature. It can be noted that the standard degradation temperature of cellulose is 135 °C with a melting flow temperature of 240–244 °C, which will differ depending on the source of cellulose, the extraction process, and its crystal structure Podgorbunskikh, Bychkov, Ryabchikova, & Lomovsky (2020). According to TGA results in Table 1, all four samples undergo a three-step degradation process, except the cellulose complex sample containing pure hemicellulose, lignin, and cellulose (Fig. 3**(C)**). The TGA of the cellulose complex exhibited a four-stage degradation, where the glass transition temperature was identified at 300 °C (third degradation of 36.4%). However, calcination at this temperature damaged the sample due to the presence of carbon in cellulose (**Figure S.2.2.**). Hence, the second degradation phase was utilized for the preparation of pure cellulose. The first degradation (21.6%), from 25 to 100 °C, is attributed to the endothermic reaction in the sample, which leads to the evaporation of crystalline water molecules. The short second degradation (1.7%), from 100 to 200 °C, is due to the exothermic reaction in the sample, resulting in the elimination of hemicellulose and lignin, which are loosely bound to the cellulose. The third degradation (36.4%), from 200 to 310 °C, is

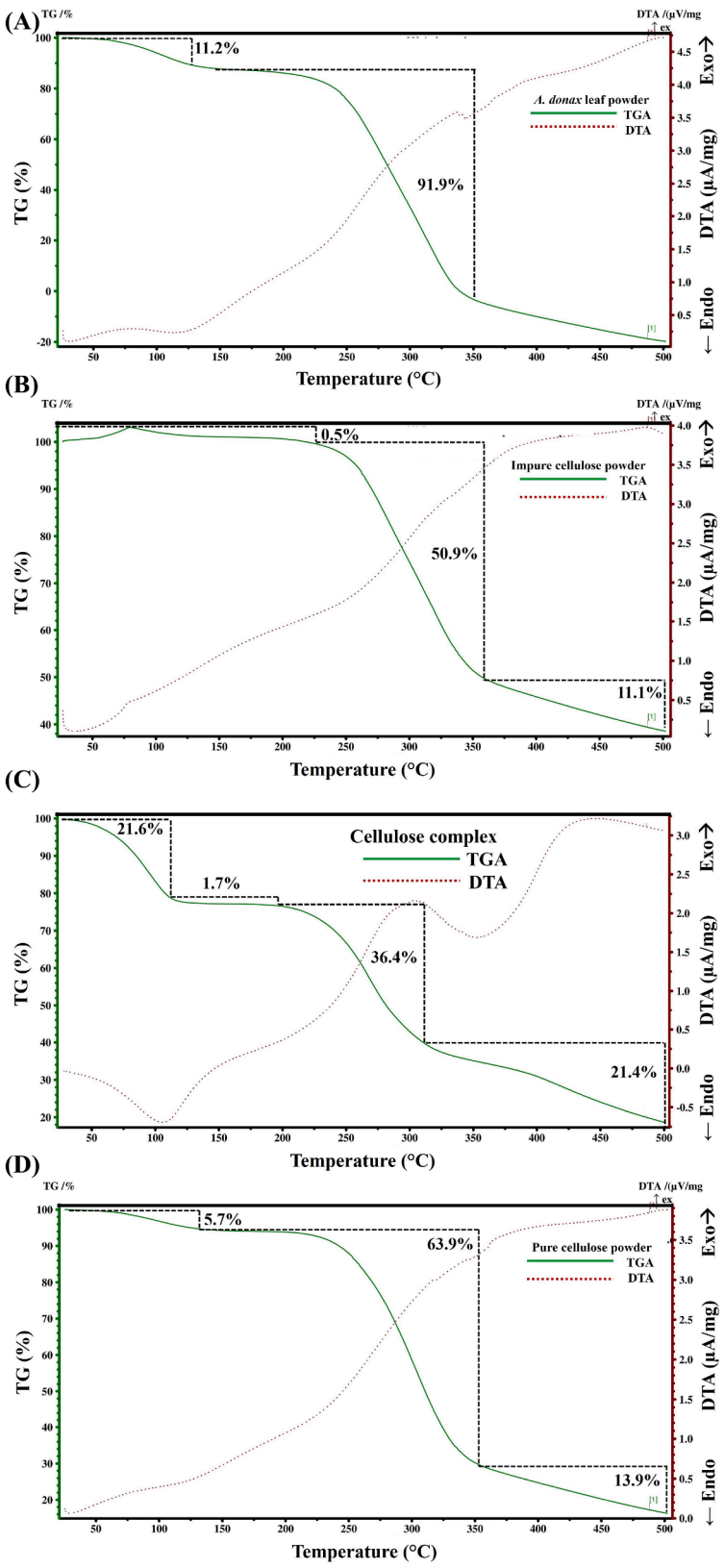

Fig. 3. TG-DTA analysis of (A) *Arundo donax* leaf extract, (B) Impure cellulose complex, (C) Cellulose complex, and (D) Pure cellulose powder.

due to an enhanced exothermic reaction, resulting in further breakdown of the cellulose structure. Since cellulose contains organic carbon material, high temperatures have caused damage to the sample (indicated by a peak in the DTA graph) Li, Qu, and Xu (2015); Pa'e, Salehudin, Hassan, Marsin, and Muhamad (2018). The final degradation (300–500 °C) led to complete degradation of cellulose, and only ash was left in the end. It can be noted (Fig. 3**(A)** and **Figure S.2.1.**) that the *A. donax* leaf powder exhibits only two degradation curves corresponding to water

Table 1
Summary of cellulose sample's TG-DTA weight loss analysis corresponding to temperature.

Sample	TGA (1st deg)	DTA (1st deg)	TGA (2nd deg)	DTA (2nd deg)	TGA (3rd deg)	DTA (3rd deg)	TGA (4th deg)	DTA (4th deg)
***A. donax* leaf powder**	25–130 °C [wl: 11.2%]	115 °C Endo	–	–	130–350 °C [wl: 91.9%]	348 °C Exo	–	–
Impure cellulose (after organosolv)	25–230 °C [wl: 0.5%]	225 °C Exo	–	–	225–355 °C [wl: 50.9%]	330 °C Exo	355–500 °C [wl: 11.1%]	485 °C Exo
Cellulose complex (after bleaching)	25–100 °C [wl: 21.6%]	102 °C Endo	101–200 °C [wl: 1.7%]	200 °C Exo	201–310 °C [wl: 36.4%]	300 °C Exo	310–500 °C [wl: 21.4%]	425 °C Exo
Pure cellulose (after calcination)	25–140 °C [wl: 5.7%]	125 °C Endo	–	–	140–355 °C [wl: 63.9%]	349 °C Exo	350–500 °C [wl: 13.9%]	495 °C Exo

Abbreviation: degradation (deg), weight loss (wl), endothermic (endo), and exothermic (exo).

and complex phytochemical as well as natural polymers (high percentage of degradation). The TG-DTA results of leaf powder were similar to the results of Ba et al., indicating that *A. donax* biomass undergoes thermal degradation from 150 to 375 °C with maximum mass loss from 325 to 340 °C at distinct heating rates (10, 15, and 20 °C/min) Ba, Liu, Wang, and Yang (2020). Further, the percentage of degradation reduces in other samples (due to the presence of natural polymers and their purity), as shown in Fig. 3 **(B-D),** resulting from organosolv, bleaching, and calcination steps. Furthermore, it can be noted that there are three degradation curves due to the thermal, evaporation of water, disintegration of carbon in the sample, and finally, cellulose into ash in the pure cellulose sample (Fig. 3**(D)**) due to the polymer rigidity (resulting from calcination process). Since cellulose is the primary natural polymer content in *A. donax*, the percentage loss in the second degradation is greater in each step with less final product yield (Table 1 and **Figure S.2.1.**). The thermal degradation of leaf powder to pure cellulose powder is similar to the bacterial cellulose as synthesized by Pa'e et al. (2018). Thus, 200 °C has been selected to yield pure cellulose structures (without lignin and hemicellulose) after calcination for 2 h. This optimal duration of calcination was identified by DLS analysis (Section 3.2), whereas the existence of cellulose in all the samples was confirmed with XRD analysis (Section 3.3).

3.2. Dynamic light scattering analysis of cellulose particles

Table 2 summarizes the DLS results showing hydrodynamic size, polydispersity index (PDI), and zeta potential of different samples with cellulose after organosolv, bleaching, and calcination processes (**Section S.3.**). It can be noted that previous studies used mechanical mills to reduce the size of the whole *A. donax* biomass, mechanically shredded into 0.5 – 4 mm of particles, that can be utilized for cellulose extraction to produce paper. Thus, the present study is a pioneering work in utilizing DLS analysis for the study of their particle size Ferrandez-García, Ferrandez-Garcia, Garcia-Ortuño, Ferrandez-Garcia, & Ferrandez-Villena (2020). The results in the present study revealed that the impure cellulose powder after the organosolv process possessed a size of 458.7 nm with PDI of ~0.5 and a zeta potential of −19.4 mV. The larger hydrodynamic size with PDI indicating polydispersity with high zeta potential may be due to the existence of several phytocompounds along with hemicellulose, cellulose, and lignin. The removal of acidic impurities and other phytocompounds during the bleaching process has led to a reduction in their hydrodynamic size with a slight decrease in PDI and an increase of the particle stability in solution, as well as a decrease in the overall zeta potential value. Later, the calcination temperature of 200 °C was selected based on TG-DTA analysis of bleached samples, which were calcined for 1, 2, and 3 h. The DLS results revealed that the hydrodynamic size of the sample calcined for 2 h is lower compared to 1 and 3 h, with comparatively lower PDI and higher zeta potential value (−32.5 mV). It can be noted that the rise in calcination time has led to a more negative charge to the particles, indicating the purity and stability of cellulose in an aqueous medium, which can be improved by increasing the calcination time from 1 to 2 h. In comparison, 3 h has led to more polydispersed particles. Further, the size, PDI, and zeta potential of pure cellulose powder obtained in this study after calcination are similar to a survey conducted to extract cellulose from eggplants Bahloul et al. (2021). FTIR analysis and UV–Visible spectroscopy analysis were also conducted to confirm the efficiency of calcination time at 2 h to yield pure cellulose powders (**Section S.4.**). However, the size is still too large to be called nanocellulose. Thus, more optimization process is required for the synthesis of nanocellulose from the cellulose.

3.3. DLS analysis of nanocellulose via fractional centrifugation approach

The centrifugal fractionation process was utilized to separate smaller-sized cellulose particles from the larger cellulose particles Zhai, Kim, Kim, & Kim (2020). Centrifugation at 5590 g of RCF was carried out for 1, 5, 10, 20, 30, and 60 min to identify the best centrifugation time, determined by DLS analysis as shown in Fig. 4 for the separation of nanocellulose (and **Section S.5**). Later, DLS analysis was performed for 20 min at different RCFs (5590, 8050 and 10,188 g) and the results are listed in **Section S.5**. The results revealed that the fractional centrifugation of 8050 g of RCF for 20 min is required to yield smaller-sized cellulose nanoparticles with high aqueous stability. The zeta potential

Table 2
DLS results of samples after organosolv, bleaching, and calcination processes.

Sample	Calcination temperature	Calcination time	Size by number in % (d. nm) ± SD	PDI ± SD	Zeta potential (mV) ± SD
Impure cellulose powder (after organosolv)	–	–	458.7 ± 0.23 (31.9%)	0.534 ± 0.23	−19.4 ± 0.09
Pure cellulose complex (after bleaching)	–	–	78.82 ± 0.18 (35.5%)	0.522 ± 0.18	−27.7 ± 0.14
After calcination at different durations					
Pure cellulose	200 °C	1 h	396.1 ± 0.06 (29.0%)	0.571 ± 0.06	−29.5 ± 0.22
Pure cellulose	200 °C	2 h	141.8 ± 0.12 (24.7%)	0.444 ± 0.12	−32.5 ± 0.19
Pure cellulose	200 °C	3 h	396.1 ± 0.31 (33.7%)	0.692 ± 0.31	−33.6 ± 0.02

*SD – Standard deviation.

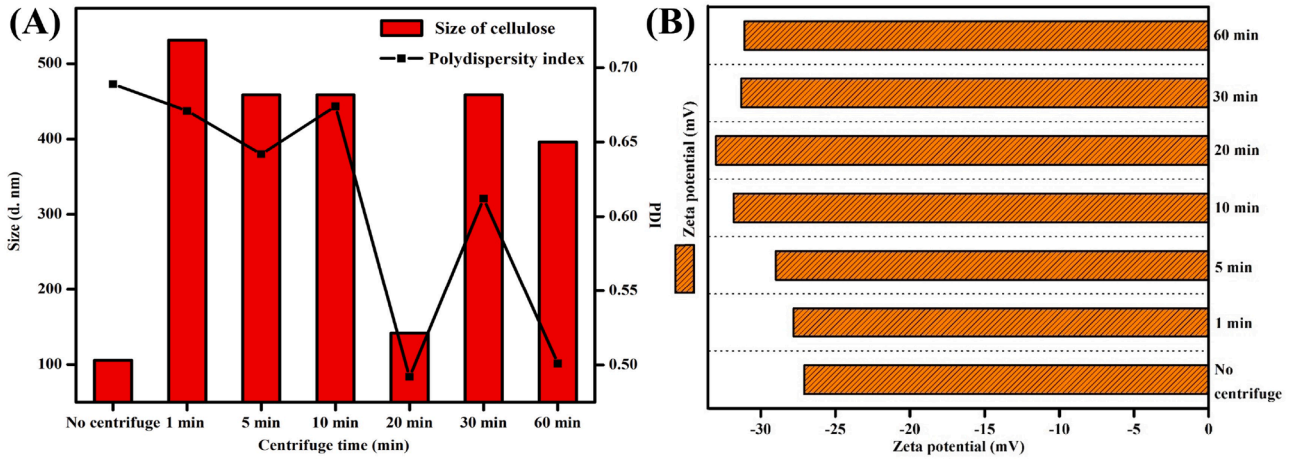

Fig. 4. Optimization of fractional centrifugation process to yield smaller-sized particles. (A) Particle size distribution by number and PDI by DLS; and (B) Zeta potential by ELS.

results of the present study were identified to be similar to those of the previous study conducted by Rashid and Dutta. However, the average particle size and PDI of nanocellulose prepared from rice grain husks were higher compared to the current study Rashid & Dutta (2020).

3.4. Crystallinity analysis of cellulose samples

The XRD results, as shown in Fig. 5, revealed that the characteristic peaks at 16° and 21° (intense peaks) denotes the presence of cellulose in all the samples. The XRD results of raw leaf powder, impure cellulose, crude cellulose powder, and pure cellulose from the present study were similar to those of raw fiber, acid treated, and bleached in the previous study conducted by Chirayil et al. (2014). The XRD peaks at 35°, 40.5°, and a few peaks at 28°−31° correspond to the presence of excess hydrogen or oxygen in the crystal lattice due to the addition of ethanol, water, and sulfuric acid during the organosolv process. Later, these minor peaks are suppressed in pure crude cellulose as the samples were bleached with sodium carbonate and hydrogen peroxide, whereas pure cellulose presents these peaks with high intensity, indicating the purity of the cellulose, which contains more hydrogen and oxygen in the sample Jiang JiaHao & Wang XiWen (2019); Keshk & Hamdy (2019). However, it is noteworthy that the XRD peak corresponds to the cellulose complex that exists in the sample, which is comprised of cellulose, hemicellulose, and lignin Gebresemati, Gabbiye, & Sahu (2017); Syazwani, Efzan, Kok, & Nurhidayatullaili (2022). Nanocellulose was extracted using the fractional centrifugation method, collecting the supernatant, which contains nanocellulose in colloidal form. Therefore, the silica base was used as a reference. The colloidal sample was then added for analysis. The graph comparing the silica base and nanocellulose in silica base showed that the silica base does not exhibit any peaks, while the nanocellulose sample showed a peak at 29° (**Section S.6.**). All other peaks are suppressed due to the presence of water and the characteristic peak at 21° was shifted to 29° as the presence of liquid suppresses the X-ray signals. A similar shift in the nanocellulose peak towards the right in the present study was also observed in a previous work, where nanocellulose was prepared using citrus waste biomass Mahdy et al. (2024); Mariño, Lopes da Silva, Durán, & Tasic (2015). However, it is evident that the sample contains cellulose, and the peaks indicate an amorphous nature due to the interaction of water within the sample.

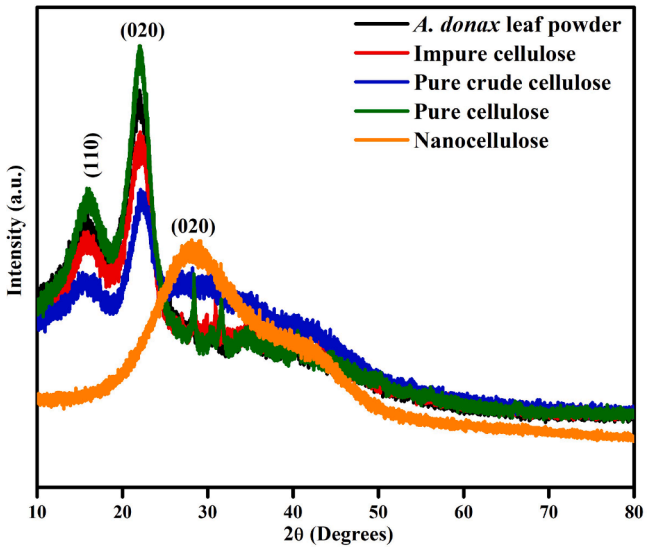

Fig. 5. XRD spectroscopy analysis to identify crystallinity of *A. donax* leaf powder, impure cellulose (after organosolv process), pure crude cellulose (after bleaching), pure cellulose (after calcination) and nanocellulose (after fractional centrifugation).

3.5. Functional group analysis of cellulose samples

The colloidal nanocellulose sample was added (one drop) in the potassium bromide (KBr) pellet to analyze the sample (the KBr method was used as the amount of freeze-dried nanocellulose powder was limited (10 mg/mL) to analyze XRD). Thus, FTIR spectra of pure KBr pellet (reference) and pellet with nanocellulose are included in supplementary information **Section S.7.** All other samples were analyzed using the attenuated total reflectance (ATR) method. It can be noted from Fig. 6 (and **Table S.7.1.**) that the peaks in the cellulose complex are absent and shifted in pure cellulose, indicating that the calcination temperature has removed hemicellulose and lignin leading to the formation of cellulose and nanocellulose Bessa et al. (2020). The peak shifts in the FTIR spectra were also similar to those observed in the pure bacterial cellulose analyzed recently by Kostryukov et al. (2023). Furthermore, several vibrational signals are present in *A. donax* leaf powder due to the presence of various natural polymers and phytochemicals in the sample, as previously reported (Ammari, 2014; Martínez-Sanz et al., 2018), which were reduced to only three peaks in nanocellulose. In each step, the processes (organosolv, bleaching, calcination, and centrifugation) led to the elimination of components (its functional groups) and the formation of nanocellulose.

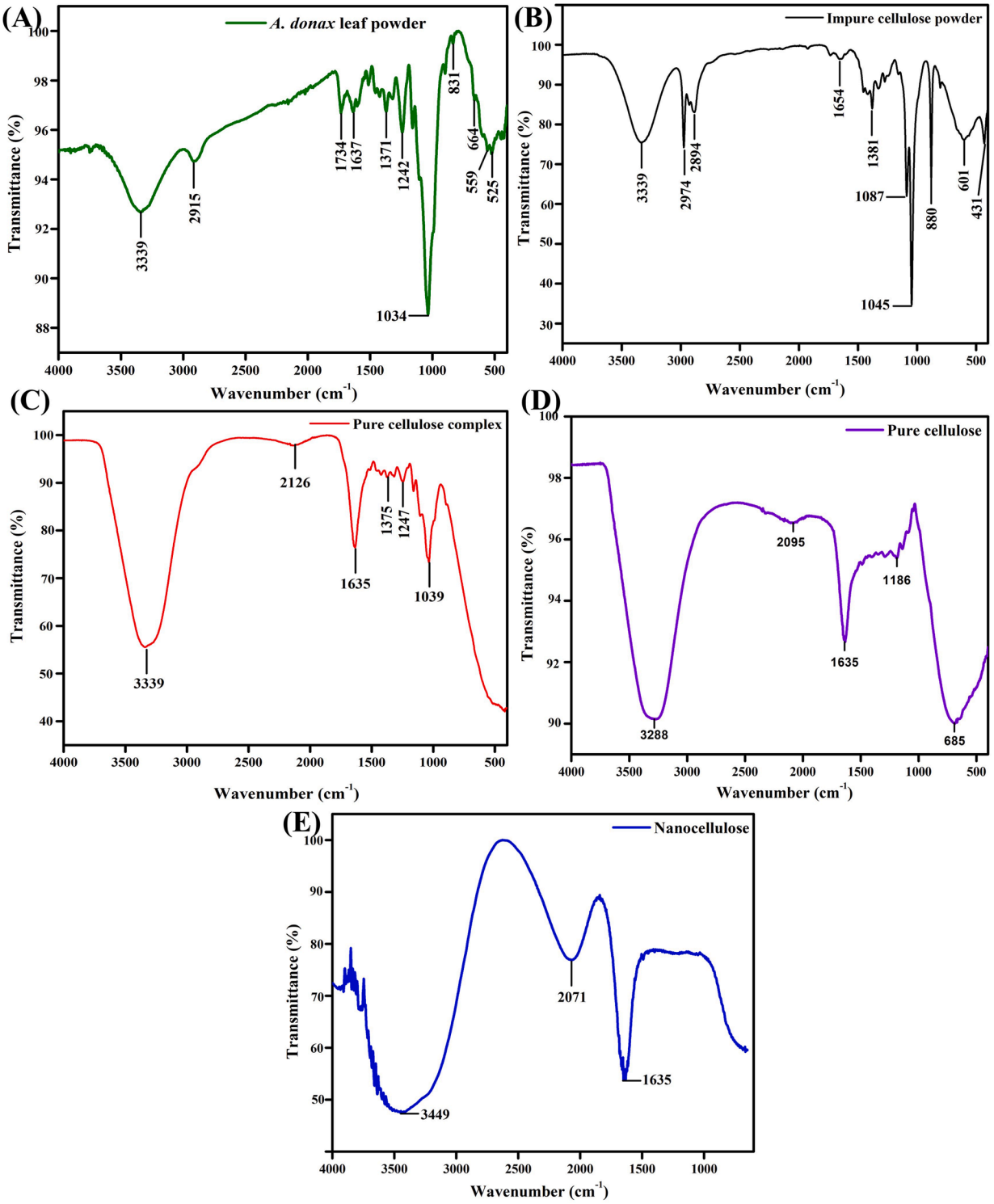

Fig. 6. Functional group analysis via FTIR spectra of (A) *A. donax* leaf powder, (B) impure cellulose (after organosolv process), (C) pure crude cellulose (after bleaching), (D) pure cellulose (after calcination), and (E) nanocellulose (after fractional centrifugation).

3.6. Optical studies of cellulose samples at different stages

The peak at 292 nm, as shown in Fig. 7, represents the presence of oxygen in the sample, as the terminal structure of cellulose contains oxygen. The peak at 282–284 nm indicates the presence of a carbon-hydrogen-oxygen (CH_2OH) bond in the structure of cellulose in impure and pure cellulose complexes. The peak shift from 284 nm to 282 nm in impure cellulose to pure cellulose complex indicates that the bleaching and washing processes has yielded a pure cellulose complex containing cellulose, hemicellulose, and lignin polysaccharides. The shift from 282 to 284 nm to 281 nm and 280 nm is attributed to the conversion of the cellulose complex to pure complex Farooq et al. (2020); Shukla, Dubey, Ashutosh Tiwari, & Bharadvaja (2013). Furthermore, the peak in nanocellulose is reduced to 290 nm, indicating a reduction in size without any peaks observed at 284–282 nm. The UV–visible spectral analysis of nanocellulose shows a specific absorption

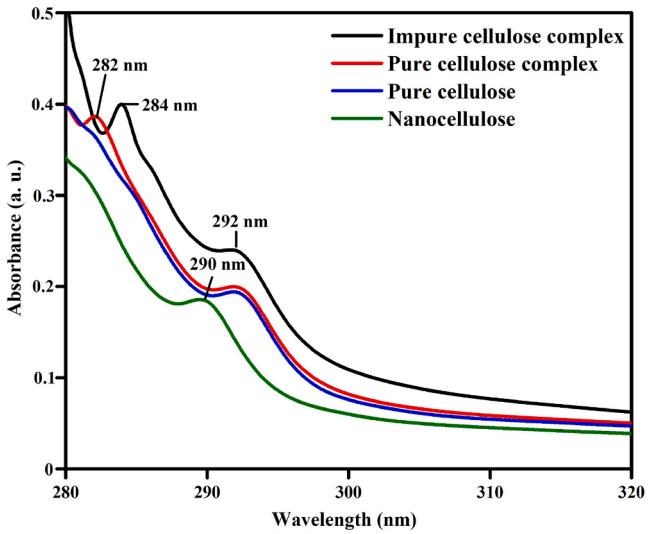

Fig. 7. UV-visible spectroscopy data of impure cellulose complex (after organosolv process denoted as impure), pure crude cellulose (after bleaching), pure cellulose (after calcination), and nanocellulose (after fractional centrifugation).

band at 290 nm that is similar to the one observed in the previous study conducted by Gond et al. Gond, Gupta, & Jawaid (2021).

3.7. Morphology analysis of cellulose nanoparticles (nanocellulose)

The SEM images, as shown in Fig. 8 at different scales, demonstrate that the freeze-dried nanocellulose exists within the fibrous matrix. One can also see a combination of several smaller particles with certain larger particles, which indicates their polydispersity due to the freeze-drying process. It is possible to observe, within the fibrous matrix, that the nanocellulose particles have distinct shapes, such as spherical and other more elongated structures. The size appears larger in SEM analysis, compared to DLS data, due to the freeze-drying process, where different shapes are integrated. The morphology of the nanocellulose is similar to the fibrous cellulose nanoparticles isolated from *A. donax* prepared by Martinez-Sanz et al. Martínez-Sanz et al. (2018). Further, the existence of spherical cellulose nanoparticles in the present study, along with fibrous cellulose structures (Doan & Chiang, 2022), was also similar to the one obtained by Meyabadi et al. Meyabadi, Dadashian, Sadeghi, & Asl (2014).

3.8. Gelatin hydrogel formulation of nanocellulose

It has been observed that the gel rigidity is high when a high volume of gelatin and a low volume of nanocellulose are mixed. Thus, the hydrogel samples with 18 mL of gelatin and 2 mL of nanocellulose were selected based on systematic characterization-based optimization.

3.8.1. UV–Visible spectral analysis to determine nanocellulose release kinetics from hydrogels

The 1 × 1 cm ballistic gelatin hydrogel samples (sample details in the supplementary information **Section S.8.** and **S.9.3.**) were immersed in 3 mL of ultrapure water, and their UV–Visible absorbance was analyzed for over 3 days to evaluate the release of nanocellulose. Nanocellulose showed absorbance at 290 nm, whereas pure gelatin at 292 nm, as shown in Fig. 9 (data in **Section S.9.**). It is noteworthy that the hydrogel samples with decreasing gelatin hydrogel content (18–10 mL) and an increase in the nanocellulose (2–10 mL) showed an increase in the absorbance at 292 nm. This is due to the interaction of nanocellulose whitin the polymer network of gelatin during gel formation Maharana & Misra (2018). When the samples were in water, the hydrogel was transparent, allowing for the proper acquisition of UV–Visible spectra. It is also noticeable that the absorbance of pure gelatin increases until day 2 and reduces on day 3. When the volume of gelatin reduces, the absorbance value increases (except for sample 3), indicating that the nanocellulose is strongly bound in the gelatin hydrogel. When the in-water spectra of nanocellulose released from gelatin were observed, all samples yielded a maximum at 292 nm, indicating that the morphology of released nanocellulose is modified due to the interaction of polymers in the hydrogel. The absorbance of sample 1 with 18 mL of gelatin is higher than that of pure gelatin hydrogel, indicating the presence of nanocellulose. On day 0, the absorbance of the nanocellulose hydrogel sample increased (except for sample 3), with a decrease in gelatin volume in the sample. Thus, sample 3 can be considered a threshold point, and further decrease in the gelatin volume may lead to weaker gels, that could increase the nanocellulose release along with gelatin in water. Hence, samples 1 and 2 were identified as releasing more nanocellulose and were selected for further analysis.

3.8.2. Swelling test of gelatin hydrogel-nanocellulose samples in water

The swelling test of gelatin hydrogel samples was measured by adding 3 mL of water. The weight of the hydrogel in each stage is detailed in supplementary information **Section S.10**. When the gel swells in the water (polymer chains absorb water and loosen), it releases nanocellulose and loses its weight, as shown in **Table S.10.2**. It can be noted from Fig. 10 that pure gelatin swelled more on day 1 and less on day 2 and showed no swelling on day 3. Sample 1, with a higher gelatin volume and less nanocellulose, swelled more on day 2 than on day 1, whereas sample 4 swelled the most on day 1. Sample 4 swelled more, and slow swelling was observed in sample 1, compared to other samples, which is essential for the controlled release of nanocellulose. However, the swelling capacity of the ballistic hydrogel prepared in this work is lower than that in previous reports Pal, Banthia, & Majumdar (2007); Yousefi-Mashouf, Bailly, Orgéas, & Henrich Bernardoni (2023) due to the addition of nanocellulose, which could be improved by increasing the gelatin content in the future. Thus, sample 1 was selected for further analysis.

3.8.3. DLS analysis of optimized gelatin-formulated nanocellulose at different temperatures

The study showed that the gelatin hydrogel sample above 25 °C (35–55 °C) disintegrated and released along with the nanocellulose. Thus, the size varies randomly, which is also indicated in their zeta potential data, as shown in Fig. 11 Jiang YaNi et al. (2018). The release of nanocellulose from the gelatin hydrogel is remained stable at 25 °C as shown in the supplementary information **Section S.11**. The temperature vs size studies showed that all the hydrogel samples disintegrated after 35 °C, as revealed by the zeta potential results. Also, it can be noted that the hydrogel with a high volume of gelatin and less volume of nanocellulose (sample 1 with 18 mL of gelatin and 2 mL of nanocellulose) remained relatively stable until 45 °C, compared to other samples and control Du et al. (2019). The hydrodynamic properties of the hydrogel with nanocellulose in the present study (from 25–55 °C) are similar to those of pure gelatin reported in the literature Bertsch, Andrée, Besheli, & Leeuwenburgh (2022); Bohidar (1998). The size of the particles released is smaller (nanocellulose: average size is 91.2 nm, 0.428 PDI, and zeta potential of −35.5 mV) due to the gel releasing its content slowly depending on its permeability. However, the difference in zeta potential and PDI indicates that the temperature affects the stability of the gel and causes the nanocelluloses to be released slowly Gabriel, Belete, Hause, Neubert, & Gebre-Mariam (2022). It is noteworthy that the pure gelatin gel possesses a positive charge until 25–45 °C, which was altered to a negative charge at 55 °C. Conversely, the addition of nanocellulose in gelatin gel altered its surface charge (negative at low temperature, switching to positive charge at high temperature). In particular, these changes are prominent in samples 1 and 2 (low nanocellulose content), whereas samples 3–5 (high nanocellulose content) possess slightly altered zeta potential. The stability (zeta potential via

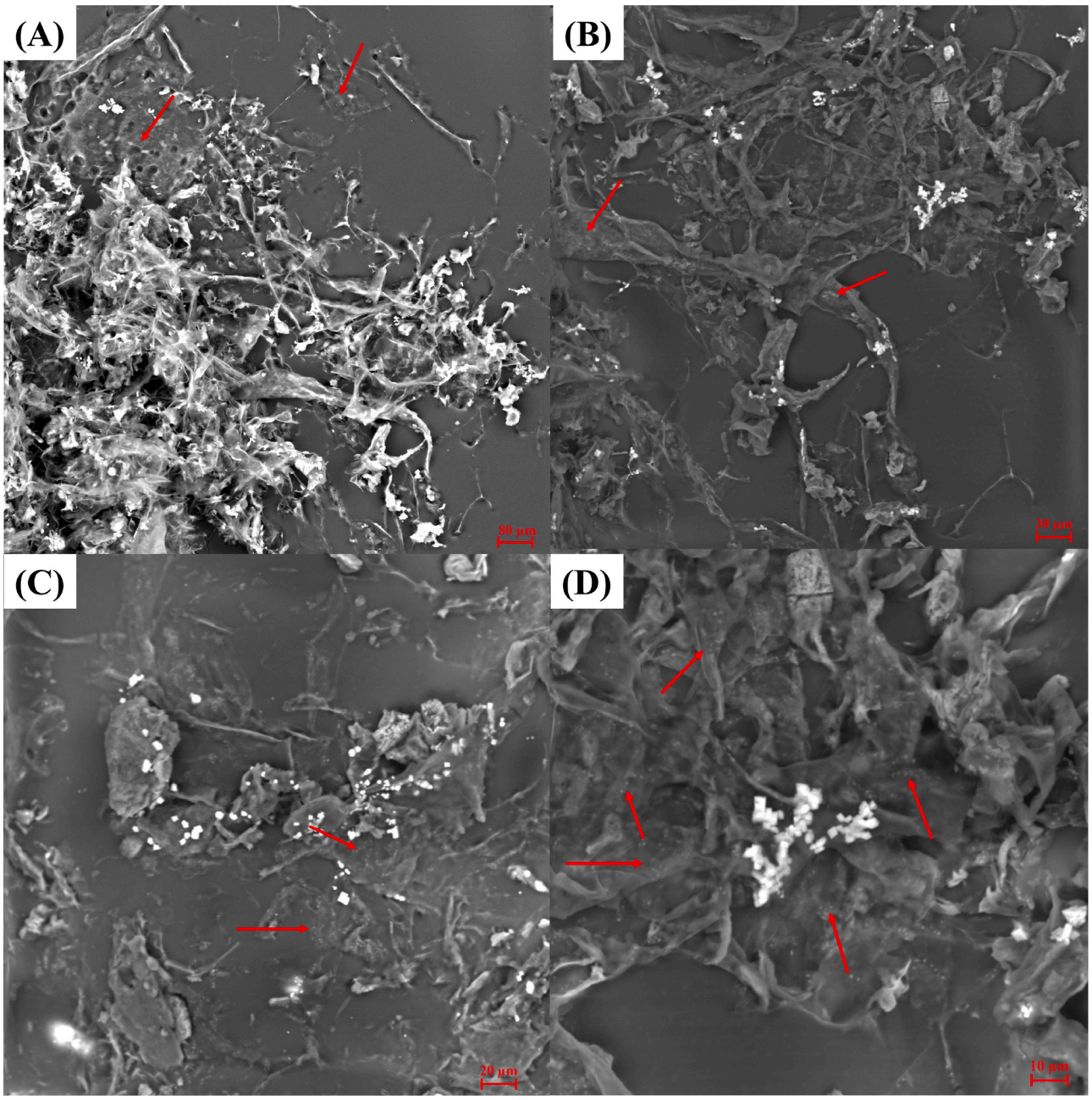

Fig. 8. Morphological analysis using scanning electron microscope (SEM) of freeze-dried nanocellulose sample at different scales of (A) 80 µm; (B) 30 µm; (C) 20 µm and (D) 10 µm.

surface charge) of the gel at different temperatures (low to high) indicates their ability to withstand high temperatures (55 °C) depending on nanocellulose content in the gel, compared to room temperature.

Nevertheless, it has been observed that the gel withstands its moderate structural rigidity until 55 °C, especially in pure gelatin gel samples 1 and 2. Moreover, samples 3–5 degraded a little after 45 °C due to higher nanocellulose and lower gelatin content. The gel samples were also subjected to pH alterations. The gel samples are neutral (6.8 pH), and a slight change in pH (acidic/basic) affects their stability, causing the gel to degrade . As a result, the gel samples were easily disintegrated in a biological system, even with slight pH changes. Therefore, sample 1 was selected for further analysis without any pH alterations.

3.8.4. TG-DTA-based thermal degradation analysis of gelatin hydrogel-nanocellulose samples

Table 3 shows the TG-DTA analysis of gelatin hydrogel-nanocellulose samples under temperature-dependent degradation from 30 to 180 °C (**Section S.12.**). It can be noted that the weight loss and DTA data of pure gelatin gel differ from those of nanocellulose-formulated gelatin hydrogel samples. Among the gelatin hydrogel samples, sample 1 shows better results as it can withstand up to 152 °C in the second degradation, with less weight loss of 76% and with a maximum of 7.2% of weight loss (due to water evaporation) in the first degradation, compared to other samples. The thermal stability of sample 1 is better than that of pure gelatin, based on TG-DTA analysis, and is similar to that of the gelatin-hydroxyapatite nanocomposite Ran, Hu, Chen, Shen, & Tong (2017); Sadeghi, Zebarjad, Khademi, & Bagherzadeh (2022).

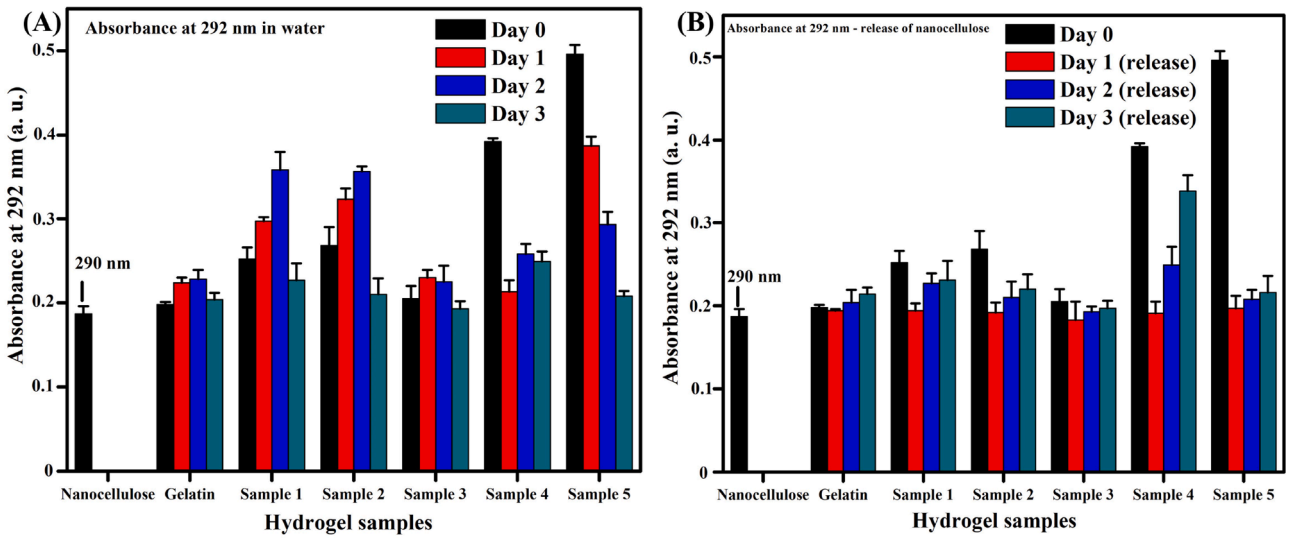

Fig. 9. (A) UV–Visible absorbance of gelatin hydrogel at 292 nm and (B) UV–Visible absorbance of gelatin hydrogel at 292 nm to identify the release kinetics of nanocellulose in water. Number of replicates – 3.

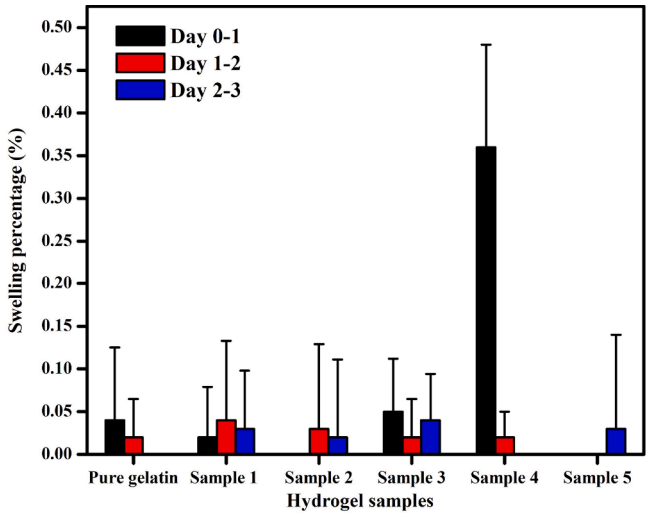

Fig. 10. Swelling percentage of gelatin samples in water. Number of replicates – 3.

3.8.5. Crystallinity analysis of gelatin hydrogel-formulated nanocellulose sample

Fig. 12 displays the XRD analysis to exhibit the crystallinity of gelatin hydrogel-formulated nanocellulose samples (data in supplementary information **Section S.13**). Gelatin is a polymer with an amorphous nature (without crystallinity), which is evident in its blunt or narrow peak in the XRD spectra Christanti & Walker (2001); Vineis et al. (2021). The addition of nanocellulose (2 mL) with 18 mL of gelatin to form sample 1 hydrogel results in specific peaks related to pure cellulose, as the hydrogel formation would have led to the agglomeration of nanocellulose. Later, the peaks in samples 2–5 related to nanocellulose gradually disappear, and the amorphous characteristic of gelatin takes over. Thus, sample 1 was selected for further studies.

3.8.6. Time vs. released nanocellulose average particle size analysis

Initially, the gelatin-nanocellulose ballistic hydrogel sample 1 (gelatin – 18 mL and nanocellulose – 2 mL) of 1 × 1 cm was immersed in 3 mL of ultrapure water for DLS analysis to evaluate the release kinetics of nanocellulose into the water. The DLS analysis of ultrapure water showed a PDI of 0.884, an average particle size of 164.2 ± 0.12 nm, and a zeta potential of 0.114 at 25 °C, which may be due to smaller bubbles formed during the analysis (**Section S.14**). The hydrogel sample (18 mL – gelatin and 2 mL – nanocellulose) was immersed in the cuvette with 3 mL of ultrapure water, where the DLS analysis was performed every 1 h for 5 h and later evaluated for 24 h and 48 h, as shown in **Figure S.15.0.**. The nanocellulose has a higher tendency for agglomeration in water (the control is ultrapure water without a gelatin sample). It can be noted that the nanocellulose is bound to the polymeric network of gelatin. Initially, the gelatin hydrogel swells in ultrapure water until 1 h, releasing nanocellulose and agglomerates, which is indicated by the average particle size of the released nanocellulose. Seo et al. (2020). After 1 h, the swelling slowly reduces, and the pores become smaller, which releases a small amount of nanocellulose (data in supplementary information **Section S.15.**). At 3 and 4 h, the released nanocelluloses are smaller in size Auvinen et al. (2020); Dash, Foston, & Ragauskas (2013). Even after analyzing for 48 h, the average particle size is below 100 nm (the nanocellulose size in ultrapure water is ~92 nm). **Figure S.9.3** shows that even after 48 h, the gelatin gel is still rigid without any visible disintegration. Thus, this analysis showed that the nanocellulose released from the gelatin hydrogel remains almost constant until 48 h without disintegration at 25 °C.

3.9. Alpha-amylase inhibition activity of standalone nanocellulose and gelatin hydrogel-formulated nanocellulose sample

The salivary alpha-amylase enzyme is utilized to convert the carbohydrate and starch to glucose/maltose/fructose, and its inhibition will reduce the blood sugar level in diabetic patients Kaur et al. (2021); Taslimi & Gulçin (2017). Ammulu et al. described the amylase inhibition assay, which was utilized in the current study with certain modifications Ammulu et al. (2021). This study evaluated the ability of nanocellulose and gelatin-formulated nanocellulose hydrogel to inhibit alpha-amylase enzyme activity. Fig. 13 shows the alpha-amylase inhibition activity of standalone nanocellulose and gelatin hydrogel-formulated nanocellulose samples. The study showed that the nanocellulose exhibits concentration-dependent enzyme inhibition activity up to 80 μg/mL (Nsor-Atindana et al., 2019), while its activity is reduced at 100 μg/mL, indicating that high concentrations leads to the agglomeration of nanocellulose, which can eventually reduce their enzyme inhibition performance Dasan, Bhat, & Ahmad (2017). In general, the amylase inhibition activity of a sample over 24 h is identified by adding an amylase inhibitor and allowing the sample react with the enzyme. However, one have also mixed the sample with NaCl for 24 h to

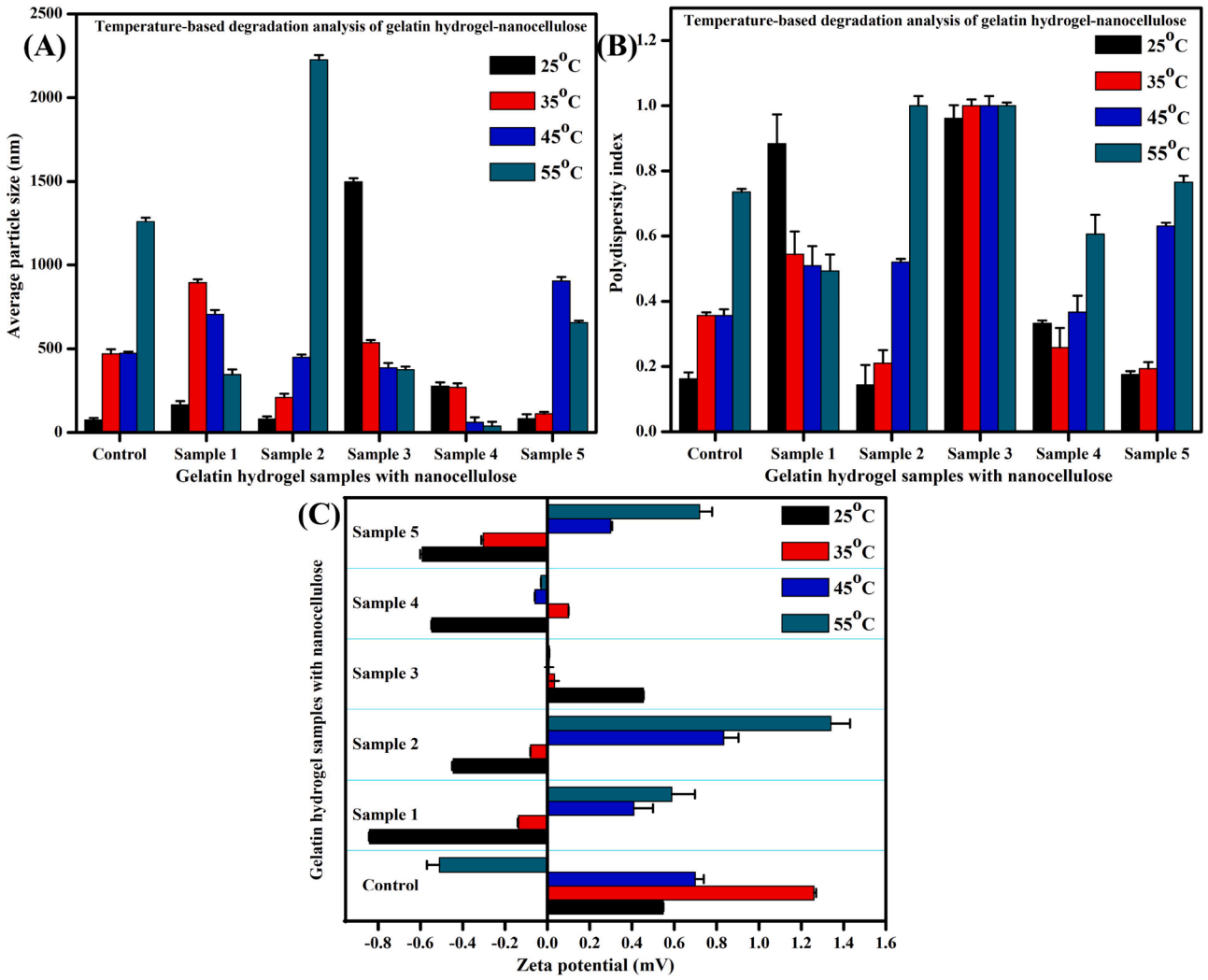

Fig. 11. Average particle size, PDI, and zeta potential values determined by DLS/ELS analysis during temperature-dependent degradation of gelatin hydrogel-formulated nanocellulose samples. Control: pure gelatin gel without nanocellulose in water. Number of replicates – 3.

Table 3
TG-DTA analysis of gelatin hydrogel sample's temperature-dependent degradation (deg: degradation; wl: weight loss (%)). *All samples experienced degradation up to 100 °C due to water reduction.

Sample name	TGA (1st deg) (°C)	TGA (2nd deg) (°C)	DTA (°C)	Inference
Sample 1	105 7.2%	152 76%	140	* and later, gel degrades (endothermic up to 140 °C).
Sample 2	100 5.5%	150 80.8%	145	* and later, gel degrades (endothermic up to 145 °C).
Sample 3	100 6.6%	142 78.6%	138	* and later, gel degrades (endothermic up to 138 °C).
Sample 4	100 5.5%	165 81.5%	155	* and later, gel degrades (endothermic up to 155 °C).
Sample 5	100 5.5%	162 84.4%	151	* and later, gel degrades (endothermic up to 151 °C).
Pure gelatin gel (control)	100 6.1%	162 79%	146	* and later, gel degrades (endothermic up to 146 °C).

determine the the sample's ability to reduce the catalytic effect of NaCl or starch substrate, which eventually reduces the binding sites of the enzymes/their binding activity. The results showed that the activity was better than that of the control group. Furthermore,

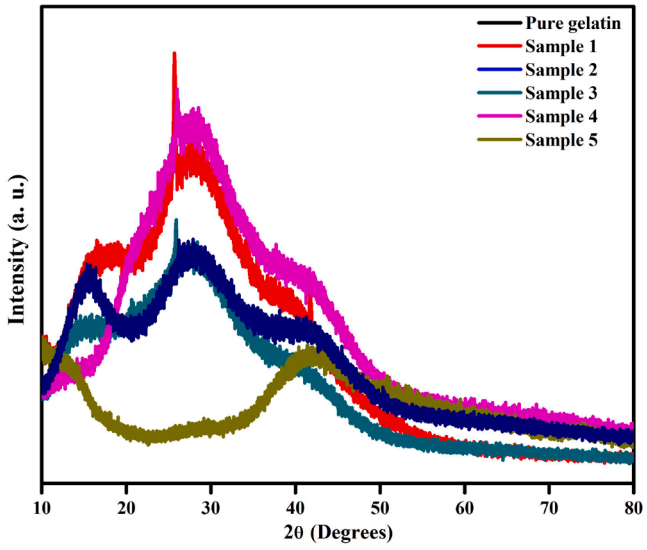

Fig. 12. XRD analysis of gelatin hydrogel-formulated nanocellulose sample.

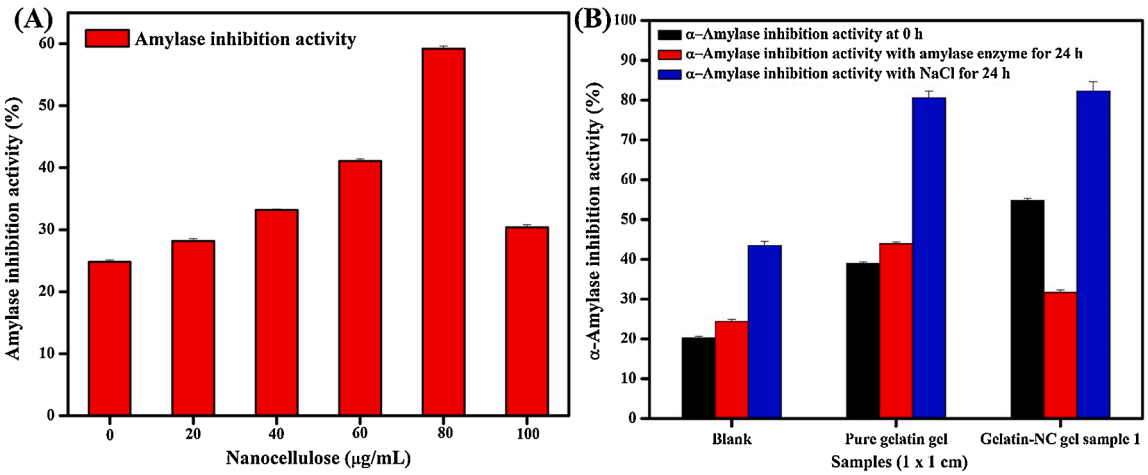

Fig. 13. Alpha-amylase inhibition activity of (A) standalone nanocellulose (NC) and (B) pure gelatin hydrogel and gelatin hydrogel (18 mL) formulated nanocellulose (2 mL) [Sample 1] at 0, 24 h and with sodium chloride as catalyst for 24 h.

nanocellulose-containing gelatin gel (sample 1) possesses enhanced enzyme inhibition activity at 0 h, compared to pure gelatin gel. It should be noted that the reaction of the samples with NaCl for 24 h has led to approximately ~80% and 82% enzyme inhibition by pure gelatin and gelatin-nanocellulose hydrogel, respectively. This indicates that the reaction prior to adding amylase has led to the disruption of substrate or catalyst (NaCl) by the synergistic effect of gelatin and nanocellulose Kaur et al. (2021); Lassoued et al. (2015). This may have led to the absence of binding sites required for amylase to convert the starch into maltose. The alpha-amylase inhibition activity of the gelatin-formulated nanocellulose hydrogel in this study is better than the enzyme inhibition ability of standalone nanocellulose Li, Liang, Huang, Huang, & Feng (2022); Nsor-Atindana et al. (2020); Nsor-Atindana et al. (2019). These results represent a step forward when formulating this gel into antidiabetic gummies. At 0 h, the release of nanocellulose will inhibit the binding site of the enzyme, which was increased at 24 h, indicating the sustainable release of nanocellulose. The study also shows a different aspect of nanocellulose: instead of effectively inhibiting enzyme directly, nanocellulose combined with gelatin possesses the ability to block the binding site of catalyst and starch substrate, which eventually halts the enzyme's activity to convert starch to maltose.

4. Conclusion

In this study, cellulose was extracted from the invasive *Arundo donax* plant via an organosolv, bleaching, and calcination approach, which yielded pure cellulose that was then utilized to synthesize nanocellulose of moderately monodispersed (0.428 PDI), 91.2 nm in size and a potential zeta of −35.5 mV, indicating high stability in water. Furthermore, the resultant nanocellulose was formulated into a gelatin ballistic hydrogel for sustained release at the target site. Systematic characterization of the hydrogel samples (with different ratios of gelatin and nanocellulose) revealed that the sample with high gelatin and low nanocellulose content is thermally stable until 152 °C, nanocellulose release for 3 days with a sustained release for 48 h up to 45 °C. This study will be highly beneficial for the extraction of novel nanocellulose from invasive plants as a source, thereby reusing it for medical applications. In addition, the gelatin-formulated nanocellulose exhibited alpha-amylase inhibition activity at a dosage of 80 µg/mL, which can be a game-changer in the field of antidiabetic agents as a potential medical gummy for sustained reduction of blood glucose levels.

Declaration of competing interest

The authors declare that they have no known competing financial interests or personal relationships that could have appeared to influence the work reported in this paper.

Data availability

Data will be made available on request.

Acknowledgement

This work was supported by FCT-Fundação para a Ciência e a Tecnologia (Portugal) through the CQM Base Fund - UIDB/00674/2020 (DOI: 10.54499/UIDB/00674/2020), by ARDITI-Agência Regional para o Desenvolvimento da Investigação Tecnologia e Inovação, through the project, M1420–01–0145-FEDER-000005 - Centro de Química da Madeira - CQM^{+} (Madeira 14–20 Program) and project M1420–09–5369-FSE-000002 for the post-Doc Grant of R.C. The authors acknowledge Laboratório Regional de Engenharia Civil (LREC), Madeira, Portugal, and Dr. Énio Fernandes (Senior Technician) for their support to access TG-DTA and XRD equipment. The author (J. R.) acknowledges Programa de Cooperacion Territorial INTERREG V-A MAC 2014–2020, Project Inv2Mac (MAC2/4.6d/229) for financial support, including a post-Doc Grant for J.J.

Supplementary materials

Supplementary material associated with this article can be found, in the online version, at doi:10.1016/j.carpta.2024.100575.

References

Afrin, S., & Karim, Z. (2017). Isolation and surface modification of nanocellulose: necessity of enzymes over chemicals. *ChemBioEng Reviews, 4*(5), 289–303.
Alam, M. S., & Mohd, S. (2019). A review on alpha-amylase inhibitors for the treatment of diabetes mellitus. *Think India Journal, 22*(30), 1332–1353.
Amaral-Labat, G., Szczurek, A., Fierro, V., Pizzi, A., Masson, E., & Celzard, A. (2012). "Blue glue": A new precursor of carbon aerogels. *Microporous and Mesoporous Materials, 158*, 272–280.
Amarone, N., Iovane, G., Marranzini, D., Sessa, R., Guedes, M. C., & Faggiano, B. (2023). Arundo donax L. as sustainable building material,. *Sustainable Buildings, 6*, 2.
Ammari, T. G. (2014). Utilization of a natural ecosystem bio-waste; leaves of Arundo donax reed, as a raw material of low-cost eco-biosorbent for cadmium removal from aqueous phase. *Ecological Engineering, 71*, 466–473.
Ammulu, M. A., Vinay Viswanath, K., Giduturi, A. K., Vemuri, P. K., Mangamuri, U., & Poda, S. (2021). Phytoassisted synthesis of magnesium oxide nanoparticles from Pterocarpus marsupium rox. b heartwood extract and its biomedical applications. *Journal of Genetic Engineering and Biotechnology, 19*(1), 1–18.
Auvinen, V.-V., Virtanen, J., Merivaara, A., Virtanen, V., Laurén, P., Tuukkanen, S., & Laaksonen, T. (2020). Modulating sustained drug release from nanocellulose

hydrogel by adjusting the inner geometry of implantable capsules. *Journal of Drug Delivery Science and Technology, 57*, Article 101625.
Ba, Y., Liu, F., Wang, X., & Yang, J. (2020). Pyrolysis of C3 energy plant (arundo donax): Thermogravimetry, mechanism, and potential evaluation. *Industrial crops and products, 149*, Article 112337.
Bahloul, A., Kassab, Z., El Bouchti, M., Hannache, H., Oumam, M., & El Achaby, M. (2021). Micro-and nano-structures of cellulose from eggplant plant (Solanum melongena L) agricultural residue. *Carbohydrate Polymers, 253*, Article 117311.
Balea, A., Blanco, A., Delgado-Aguilar, M., Monte, M. C., Tarres, Q., Mutjé, P., & Negro, C. (2021). Nanocellulose characterization challenges. *BioResources, 16*(2), 4382.
Bermudez-Beltrán, K. A., Marzal-Bolaño, J. K., Olivera-Martínez, A. B., & Espitia, P. J. P. (2020). Cape gooseberry petit suisse cheese incorporated with moringa leaf powder and gelatin. *LWT, 123*, Article 109101.
Bertsch, P., Andrée, L., Besheli, N. H., & Leeuwenburgh, S. C. (2022). Colloidal hydrogels made of gelatin nanoparticles exhibit fast stress relaxation at strains relevant for cell activity. *Acta Biomaterialia, 138*, 124–132.
Bessa, W., Tarchoun, A. F., Trache, D., & Derradji, M. (2021). Preparation of amino-functionalized microcrystalline cellulose from Arundo Donax L. and its effect on the curing behavior of bisphenol A–based benzoxazine. *Thermochimica Acta, 698*, Article 178882.
Bessa, W., Trache, D., Derradji, M., Ambar, H., Tarchoun, A. F., Benziane, M., & Guedouar, B. (2020). Characterization of raw and treated Arundo donax L. cellulosic fibers and their effect on the curing kinetics of bisphenol A-based benzoxazine. *International Journal of Biological Macromolecules, 164*, 2931–2943.
Bohidar, H. B. (1998). Hydrodynamic properties of gelatin in dilute solutions. *International Journal of Biological Macromolecules, 23*(1), 1–6.
Boonprasertpoh, A., Chantarangkul, P., Thiangtham, S., Kitiyanan, B., Noisumdaeng, P., Wootthikanokkhan, J., & Meeyoo, V. (2024). Fabrication and characterizations of electrospun cellulose/CeO2 nanocomposite membranes. *Cellulose, 31*(5), 2957–2973.
Brosse, N., Hussin, M. H., & Rahim, A. A. (2019). Organosolv processes. *Biorefineries*, 153–176.
Carrier, M., Loppinet-Serani, A., Denux, D., Lasnier, J.-M., Ham-Pichavant, F., Cansell, F., & Aymonier, C. (2011). Thermogravimetric analysis as a new method to determine the lignocellulosic composition of biomass. *Biomass and Bioenergy, 35*(1), 298–307.
Chauhan, V. S., & Chakrabarti, S. K. (2012). Use of nanotechnology for high performance cellulosic and papermaking products. *Cellulose Chemistry and Technology, 46*(5), 389.
Chirayil, C. J., Joy, J., Mathew, L., Mozetic, M., Koetz, J., & Thomas, S. (2014). Isolation and characterization of cellulose nanofibrils from Helicteres isora plant. *Industrial Crops and Products, 59*, 27–34.
Christanti, Y., & Walker, L. M. (2001). Surface tension driven jet break up of strain-hardening polymer solutions. *Journal of Non-Newtonian Fluid Mechanics, 100*(1-3), 9–26.
Dasan, Y., Bhat, A., & Ahmad, F. (2017). Polymer blend of PLA/PHBV based bionanocomposites reinforced with nanocrystalline cellulose for potential application as packaging material. *Carbohydrate Polymers, 157*, 1323–1332.
Dash, R., Foston, M., & Ragauskas, A. J. (2013). Improving the mechanical and thermal properties of gelatin hydrogels cross-linked by cellulose nanowhiskers. *Carbohydrate Polymers, 91*(2), 638–645.
Dhali, K., Ghasemlou, M., Daver, F., Cass, P., & Adhikari, B. (2021). A review of nanocellulose as a new material towards environmental sustainability. *Science of the Total Environment, 775*, Article 145871.
Dhital, S., Gidley, M., & Warren, F. (2015). Inhibition of α-amylase activity by cellulose: Kinetic analysis and nutritional implications. *Carbohydrate Polymers, 123*, 305–312.
Doan, T. K. Q., & Chiang, K. Y. (2022). Characteristics and kinetics study of spherical cellulose nanocrystal extracted from cotton cloth waste by acid hydrolysis. *Sustainable Environment Research, 32*(1), 26.
Driesche, R. V., & Center, T. (2013). Biological control of invasive plants in protected areas. *Plant invasions in protected areas* (pp. 561–597). Springer.
Du, H., Liu, W., Zhang, M., Si, C., Zhang, X., & Li, B. (2019). Cellulose nanocrystals and cellulose nanofibrils based hydrogels for biomedical applications. *Carbohydrate Polymers, 209*, 130–144.
Eigenbrode, S. D., Andreas, J. E., Cripps, M. G., Ding, H., Biggam, R. C., & Schwarzländer, M. (2008). Induced chemical defenses in invasive plants: a case study with Cynoglossum officinale L. *Biological Invasions, 10*(8), 1373–1379.
Esmaeili, S., Dayani, L., Taheri, A., & Zolfaghari, B. (2021). Phytochemical standardization, formulation and evaluation of oral hard gelatin capsules from Pinus eldarica bark extract. *Avicenna Journal of Phytomedicine, 11*(2), 168–179.
Farooq, A., Patoary, M. K., Zhang, M., Mussana, H., Li, M., Naeem, M. A., … Liu, L. (2020). Cellulose from sources to nanocellulose and an overview of synthesis and properties of nanocellulose/zinc oxide nanocomposite materials. *International Journal of Biological Macromolecules, 154*, 1050–1073.
Ferrandez-García, M. T., Ferrandez-Garcia, A., Garcia-Ortuño, T., Ferrandez-Garcia, C. E., & Ferrandez-Villena, M. (2020). Assessment of the physical, mechanical and acoustic properties of Arundo donax L. biomass in low pressure and temperature particleboards. *Polymers, 12*(6), 1361.
Gabriel, T., Belete, A., Hause, G., Neubert, R. H., & Gebre-Mariam, T. (2022). Nanocellulose-based nanogels for sustained drug delivery: Preparation, characterization and in vitro evaluation. *Journal of Drug Delivery Science and Technology, 75*, Article 103665.
Gaikwad, A., Debnath, K., & Gupta, M. (2023). Effects of alkaline-acid treatment on the physiochemical attributes of natural cellulosic fiber of Arundo donax L. *Journal of Applied Polymer Science, 140*(48), e54724.
Gebresemati, M., Gabbiye, N., & Sahu, O. (2017). Sorption of cyanide from aqueous medium by coffee husk: Response surface methodology. *Journal of Applied Research and Technology, 15*(1), 27–35.
Gómez-Mascaraque, L. G., & Lopez-Rubio, A. (2020). Encapsulation of plant-derived bioactive ingredients through electrospraying for nutraceuticals and functional foods applications. *Current Medicinal Chemistry, 27*(17), 2872–2886.
Gond, R., Gupta, M., & Jawaid, M. (2021). Extraction of nanocellulose from sugarcane bagasse and its characterization for potential applications. *Polymer Composites, 42*(10), 5400–5412.
Gorgieva, S., & Trček, J. (2019). Bacterial cellulose: Production, modification and perspectives in biomedical applications. *Nanomaterials, 9*(10), 1352.
Hafliger, E., & Scholz, H. (1981). Grass weeds 2. Weeds of the subfamilies Chloridoideae, Pooideae, Oryzoideae. *Grass weeds, 137*, 23.
Hameed, A., Ali, F., Riaz, K., Alam, M. W., Ali, S., Rasheed, R., & Sarfraz, S. (2024). *Management Approaches for Biological Control of Invasive Species, in Plant Quarantine Challenges under Climate Change Anxiety* (pp. 435–461). Springer.
Heinze, T., El Seoud, O. A., & Koschella, A. (2018). Production and characteristics of cellulose from different sources. *Cellulose Derivatives* (pp. 1–38). Springer.
Hinkson, K. M., NeSmith, J. E., Alba, C., Durham, M., Ferrell, J., & Flory, S. L. (2024). Selective method for invasive plant removal enhances restoration. *Restoration Ecology, 32*(4), e14112.
Islam, M., Sinha, A. S. K., & Prasad, K. (2024). Organosolv delignification of rice straw cellulose fiber for functional food packaging. *Cellulose*, 1–24.
Jeevanandam, J., & Rodrigues, J. (2024). Sustainable synthesis of bionanomaterials using non-native plant extracts for maintaining ecological balance: A computational bibliography analysis. *Journal of Environmental Management, 358*, Article 120892.
Jepson, W. L. (1993). *The Jepson manual: higher plants of California* (pp. 736–738). Univ of California Press. https://doi.org/10.2307/1222569
Jiang JiaHao, J. J., & Wang XiWen, W. X. (2019). Adsorption of Hg (II) ions from aqueous solution by thiosemicarbazide-modified cellulose adsorbent. *BioResources, 14*(2), 4670–4695.
Jiang YaNi, J. Y., Xv XiaoDong, X. X., Liu DongFang, L. D., Yang Zhe, Y. Z., Zhang Qi, Z. Q., Shi HongCan, S. H., Zhao GuoQi, Z. G., & Zhou JiPing, Z. J. (2018). Preparation of cellulose nanofiber-reinforced gelatin hydrogel and optimization for 3D printing applications. *BioResources, 13*(3), 5909–5924.
Kassem, H., Ali, H. E., & Saad Zaghloul, M. (2024). Arundo donax L. in Egypt: a potentially valuable economic plant. *Advances in Basic and Applied Sciences, 3*(1), 1–20.
Kassie, B. B., Daget, T. M., & Tassew, D. F. (2024). Synthesis, functionalization, and commercial application of cellulose-based nanomaterials: A review. *International Journal of Biological Macromolecules*, Article 134990.
Kaur, N., Kumar, V., Nayak, S. K., Wadhwa, P., Kaur, P., & Sahu, S. K. (2021). Alpha-amylase as molecular target for treatment of diabetes mellitus: A comprehensive review. *Chemical Biology & Drug Design, 98*(4), 539–560.
Kaur, P., Thakur, M., Tondan, D., Bamrah, G. K., Misra, S., Kumar, P., Pandohee, J., & Kulshrestha, S. (2021). Nanomaterial conjugated lignocellulosic waste: cost-effective production of sustainable bioenergy using enzymes. *3 Biotech, 11*, 1–18.
Kavimughil, M., Leena, M. M., Moses, J. A., & Anandharamakrishnan, C. (2022). 3D printed MCT oleogel as a co-delivery carrier for curcumin and resveratrol. *Biomaterials, 287*, Article 121616.
Keshk, S. M. A. S., & Hamdy, M. S. (2019). Preparation and physicochemical characterization of zinc oxide/sodium cellulose composite for food packaging. *Turkish Journal of Chemistry, 43*(1), 94–105.
Kostryukov, S., Matyakubov, H., Masterova, Y. Y., Kozlov, A. S., Pryanichnikova, M., Pynenkov, A., & Khluchina, N. (2023). Determination of lignin, cellulose, and hemicellulose in plant materials by FTIR spectroscopy. *Journal of Analytical Chemistry, 78*(6), 718–727.
Lassoued, I., Mora, L., Nasri, R., Jridi, M., Toldrá, F., Aristoy, M.-C., Barkia, A., & Nasri, M. (2015). Characterization and comparative assessment of antioxidant and ACE inhibitory activities of thornback ray gelatin hydrolysates. *Journal of Functional Foods, 13*, 225–238.
Li, H., Qu, Y., & Xu, J. (2015). Microwave-assisted conversion of lignin. *Production of Biofuels and Chemicals with Microwave* (pp. 61–82). Springer.
Li, Y., Liang, W., Huang, M., Huang, W., & Feng, J. (2022). Green preparation of holocellulose nanocrystals from burdock and their inhibitory effects against α-amylase and α-glucosidase. *Food & Function, 13*(1), 170–185.
Liu, L., & Kong, F. (2021). The behavior of nanocellulose in gastrointestinal tract and its influence on food digestion. *Journal of Food Engineering, 292*, Article 110346.
Luo, K., Wang, Y., Xiao, H., Song, G., Cheng, Q., & Fan, G. (2019). *Preparation of convertible cellulose from rice straw using combined organosolv fractionation and alkaline bleaching, 237*. IOP Publishing, Article 052053.
Maharana, S., & Misra, P. K. (2018). Probing the Gelatin–Alkylammonium salt mixed assemblies through surface tensiometry and fluorimetry. *The Journal of Physical Chemistry B, 122*(20), 5161–5172.
Mahdy, S. Z., Amin, A. S., Abouzeid, R., Moustafa, I. MI, Youssef, A., & ELhabasha, E. S. (2024). Development and evaluation of pectin extracted from citrus sinensis peel and micro/nanocellulose from the solid fraction of citrus wastes. *Egyptian Journal of Chemistry, 67*(2), 615–623.
Mariño, M., Lopes da Silva, L., Durán, N., & Tasic, L. (2015). Enhanced materials from nature: Nanocellulose from citrus waste. *Molecules, 20*(4), 5908–5923.
Martínez-Sanz, M., Erboz, E., Fontes, C., & López-Rubio, A. (2018). Valorization of Arundo donax for the production of high performance lignocellulosic films. *Carbohydrate Polymers, 199*, 276–285.
Mathura, F., & Maharaj, R. (2024). Non-wood plants as sources of cellulose for paper and biodegradable composite materials: An updated review. *Current Materials Science: Formerly: Recent Patents on Materials Science, 17*(4), 321–335.

Meyabadi, T. F., Dadashian, F., Sadeghi, G. M. M., & Asl, H. E. Z. (2014). Spherical cellulose nanoparticles preparation from waste cotton using a green method. *Powder Technology, 261*, 232–240.
Mohamad Amini, M. H. (2024). Forest and agricultural biomass. *Plant Biomass Derived Materials: Sources, Extractions, and Applications* (pp. 271–290). Wiley.
More, R. V., Antanitta. S, V., Khonde, R., & Kandasubramanian, B. (2024). Cellulose and derivatives serving as natural, versatile and biocompatible polymers in biomedical applications. *International Journal of Polymeric Materials and Polymeric Biomaterials*, 1–15.
Nasir, M., Hashim, R., Sulaiman, O., & Asim, M. (2017). *11 - Nanocellulose: Preparation methods and applications, in Cellulose-Reinforced Nanofibre Composites* (pp. 261–276). Woodhead Publishing.
Nsor-Atindana, J., Goff, H. D., Saqib, M. N., Chen, M., Liu, W., Ma, J., & Zhong, F. (2019). Inhibition of α-amylase and amyloglucosidase by nanocrystalline cellulose and spectroscopic analysis of their binding interaction mechanism. *Food Hydrocolloids, 90*, 341–352.
Nsor-Atindana, J., Yu, M., Goff, H. D., Chen, M., & Zhong, F. (2020). Analysis of kinetic parameters and mechanisms of nanocrystalline cellulose inhibition of α-amylase and α-glucosidase in simulated digestion of starch. *Food & Function, 11*(5), 4719–4731.
Nunez-Gonzalez, N., Rodriguez, J., & Gonzalez, L. (2021). Managing the invasive plant Carpobrotus edulis: is mechanical control or specialized natural enemy more effective? *Journal of Environmental Management, 298*, Article 113554.
Ozudogru, E. A., Karlik, E., Elazab, D., & Lambardi, M. (2023). Establishment of an efficient somatic embryogenesis protocol for giant reed (Arundo donax l.) and multiplication of obtained shoots via semi-solid or liquid culture. *Horticulturae, 9*(7), 735.
Pa'e, N., Salehudin, M. H., Hassan, N. D., Marsin, A. M., & Muhamad, I. I. (2018). Thermal behavior of bacterial cellulose-based hydrogels with other composites and related instrumental analysis. *Cellulose-Based Superabsorbent Hydrogels, 1*, 763–787.
Pal, K., Banthia, A. K., & Majumdar, D. K. (2007). Preparation and characterization of polyvinyl alcohol-gelatin hydrogel membranes for biomedical applications. *Aaps Pharmscitech, 8*, E142–E146.
Pires, J. R., Souza, V. G., Gomes, L. A., Coelhoso, I. M., Godinho, M. H., & Fernando, A. L. (2022). Micro and nanocellulose extracted from energy crops as reinforcement agents in chitosan films. *Industrial Crops and Products, 186*, Article 115247.
Pires, J. R. A., Souza, V. G. L., Gomes, L. A., Coelhoso, I. M., Godinho, M. H., & Fernando, A. L. (2022). Micro and nanocellulose extracted from energy crops as reinforcement agents in chitosan films. *Industrial Crops and Products, 186*, Article 115247.
Podgorbunskikh, E. M., Bychkov, A. L., Ryabchikova, E. I., & Lomovsky, O. I. (2020). The effect of thermomechanical pretreatment on the structure and properties of lignin-rich plant biomass. *Molecules, 25*(4), 995.
Ran, J., Hu, J., Chen, L., Shen, X., & Tong, H. (2017). Preparation and characterization of gelatin/hydroxyapatite nanocomposite for bone tissue engineering. *Polymer Composites, 38*(8), 1579–1590.
Randall, R. P. (2012). *A Global Compendium of Weeds. Perth, Australia: Department of Agriculture and Food Western Australia* (p. 1124).
Rashid, S., & Dutta, H. (2020). Characterization of nanocellulose extracted from short, medium and long grain rice husks. *Industrial Crops and Products, 154*, Article 112627.
Reddy, N., & Yang, Y. (2005). Structure and properties of high quality natural cellulose fibers from cornstalks. *Polymer, 46*(15), 5494–5500.
Sadeghi, E., Zebarjad, S. M., Khademi, F., & Bagherzadeh, E. (2022). Enhancing structural strength and improving cell survival through Polycaprolactone/(gelatin/hydroxyapatite) Core-Shell nanofibers for tissue engineering. *Polymer Composites, 43*(10), 7379–7389.
Semba, J. A., Mieloch, A. A., Tomaszewska, E., Cywoniuk, P., & Rybka, J. D. (2023). Formulation and evaluation of a bioink composed of alginate, gelatin, and nanocellulose for meniscal tissue engineering. *International Journal of Bioprinting, 9*(1), 621.
Seo, M., Seo, M., Choi, S.-E., Shin, K., Lee, J. B., Yang, D.-Y., & Kim, J. W. (2020). Cellulose nanofiber-multilayered fruit peel-mimetic gelatin hydrogel microcapsules for micropackaging of bioactive ingredients. *Carbohydrate Polymers, 229*, Article 115559.
Sharma, N., Munagala, M., Rajkhowa, R., Aallardyce, B., Shastri, Y., & Agrawal, R. (2021). Nanocellulose: resources, physio-chemical properties, current uses and future applications. *Frontiers in Nanotechnology, 3*, Article 747329.
Shatalov, A. A., & Pereira, H. (2005). Arundo donax L. reed: new perspectives for pulping and bleaching. Part 4. *Peroxide bleaching of organosolv pulps, Bioresource Technology, 96*(8), 865–872.
Shukla, S. K, Dubey, C., Ashutosh Tiwari, G., & Bharadvaja, A. (2013). Preparation and characterization of cellulose derived from rice husk for drug delivery. *Advanced Materials Letters, 4*(9), 714–719.
Sindhu, K., Prasanth, R., & Thakur, V. K. (2014). Medical applications of cellulose and its derivatives: Present and Future. *Nanocellulose Polymer Nanocomposites: Fundamentals and Applications* (pp. 437–477). John Wiley & Sons.
Syazwani, N. S., Efzan, M. E., Kok, C., & Nurhidayatullaili, M. J. (2022). Analysis on extracted jute cellulose nanofibers by Fourier transform infrared and X-Ray diffraction. *Journal of Building Engineering, 48*, Article 103744.
Taslimi, P., & Gulçin, İ. (2017). Antidiabetic potential: In vitro inhibition effects of some natural phenolic compounds on α-glycosidase and α-amylase enzymes. *Journal of Biochemical and Molecular Toxicology, 31*(10), e21956.
Vineis, C., Maya, I. C., Mowafi, S., Varesano, A., Ramírez, D. S., Abou Taleb, M., Tonetti, C., Guarino, V., & El-Sayed, H. (2021). Synergistic effect of sericin and keratin in gelatin based nanofibers for in vitro applications. *International Journal of Biological Macromolecules, 190*, 375–381.
Walawska, A., Olak-Kucharczyk, M., Kaczmarek, A., & Kudzin, M. H. (2024). Environmentally Friendly Bleaching Process of the Cellulose Fibres Materials Using Ozone and Hydrogen Peroxide in the Gas Phase. *Materials, 17*(6), 1355.
Weidlich, E. W. A., Flórido, F. G., Sorrini, T. B., & Brancalion, P. H. S. (2020). Controlling invasive plant species in ecological restoration: A global review. *Journal of Applied Ecology, 57*(9), 1806–1817.
Yan, J., Zhao, J., Yang, R., & Zhao, W. (2019). Bioactive peptides with antidiabetic properties: A review. *International Journal of Food Science & Technology, 54*(6), 1909–1919.
Yang, G., Ullah, M. W., & Zhijun, S. (2021). *Nanocellulose: Synthesis, Structure, Properties and Applications, 1* p. 568). World Scientific. https://doi.org/10.1142/9781786349477_0001
Yin, O. S., Ahmad, I., & Amin, M. (2015). Effect of cellulose nanocrystals content and pH on swelling behaviour of gelatin based hydrogel. *Sains Malaysiana, 44*(6), 793–799.
Yousefi-Mashouf, H., Bailly, L., Orgéas, L., & Henrich Bernardoni, N. (2023). Mechanics of gelatin-based hydrogels during finite strain tension, compression and shear. *Frontiers in Bioengineering and Biotechnology, 10*, Article 1094197.
Zhai, L., Kim, H. C., Kim, J. W., & Kim, J. (2020). Simple centrifugal fractionation to reduce the size distribution of cellulose nanofibers. *Scientific Reports, 10*(1), 11744.
Zhai, L., Kim, H. C., Kim, J. W., & Kim, J. (2020). Simple centrifugal fractionation to reduce the size distribution of cellulose nanofibers. *Scientific Reports, 10*(1), 1–8.
Zhang, S., Cavender, G. A., & Allen, C. J. (2020). Max Bloc® Carb blocker from phaseolus vulgaris with ultra-high α-Amylase inhibitory activity for glycemic control and weight management. *Journal of Nutrition and Food Science, 3*(1), Article 100011.